

Group cohesion and passive dynamics of a pair of inertial swimmers with three-dimensional hydrodynamic interactions

Mohamed Niged Mabrouk^{*} and Daniel Floryan[†]

*Department of Mechanical Engineering,
University of Houston, Houston, TX 77204, USA*

(Dated: April 23, 2024)

arXiv:2404.13152v1 [physics.flu-dyn] 19 Apr 2024

Abstract

When swimming animals form cohesive groups, they can reap several benefits. Our understanding of collective animal motion has traditionally been driven by models based on phenomenological behavioral rules, but more recent work has highlighted the critical importance of hydrodynamic interactions among a group of inertial swimmers. To study how hydrodynamic interactions affect group cohesion, we develop a three-dimensional, inviscid, far-field model of a swimmer. In a group of two model swimmers, we observe several dynamical phases, including following, divergence, collision, and cohesion. Our results illustrate when cohesive groups can passively form through hydrodynamic interactions alone, and when other action is needed to maintain cohesion. We find that misalignment between swimmers makes passive cohesion less likely; nevertheless, it is possible for a cohesive group to form through passive hydrodynamic interactions alone. We also find that the geometry of swimmers critically affects the group dynamics due to its role in how swimmers sample the velocity gradient of the flow.

I. INTRODUCTION

The collective motion of animals can be seen in numerous examples throughout the animal kingdom [1]. A canonical example is a large fish school, which can be defined as a structured and coordinated group of swimming organisms with synchronized movements [2]. Such collective motion of swimming animals confers several benefits, including defence against predators [3–5], enhanced foraging success [6], mating success [7], and increased swimming efficiency [8]. Furthermore, groups are robust in the sense that if one individual leaves the group, the group can still retain its advantages [9]. The benefits of collective motion have even led roboticists to develop robot swarms that aim to attain similar functionality [10, 11], but maintaining a cohesive group is a difficult task that requires unique strategies to coordinate dynamically interacting individuals [12]. We are principally interested in this aspect of schooling—the cohesion of groups—especially in the role that hydrodynamic interactions play.

Since [Weihs](#)' seminal work more than 50 years ago [8], substantial work has been done

* mmabrouk@uh.edu

† dfloryan@uh.edu

to understand how inertial swimmers may harness hydrodynamic interactions between each other when schooling [13–28]. Synthesizing these studies, schooling can lead to reduced energy expenditure when swimming under the right conditions. A swimmer can reduce its energy expenditure by maintaining an appropriate phase offset between its kinematics and those of its neighbors, with the phase offset depending on the relative location of a swimmer to its neighbor. The phase relations arise as a result of direct interactions between two swimmers, or due to the interaction between a follower and the vortical wake of the leader. In dense schools, an effect similar to ground effect may arise [24]. In addition to energy savings, some of the cited works also note that schooling can increase swimming speed relative to swimming in isolation.

The hydrodynamic (and other) benefits of schooling can only be realized if the appropriate group structure is maintained. Thus, the dynamics that dictate the trajectories of freely moving swimmers become important. These dynamics are governed by the active decision-making and social interactions of swimmers [29, 30], as well as by passive hydrodynamic interactions. A substantial and important body of work on active decision-making and social interactions exists, and it has produced a variety of agent-based models for the interactions between individuals in a group [31–34]. These models range in complexity, but they tend to neglect the role of hydrodynamic interactions, which are expected to have an outsized effect on the collective motion of swimmers [35]. Here, we focus on passive hydrodynamic interactions. Considering only the hydrodynamic interactions allows us to answer whether a cohesive group can form passively, or whether feedback control is required to maintain a cohesive group. Additionally, a deeper understanding of the hydrodynamic interactions may change the inferences that one makes about social interactions between animals based on observations of groups of animals, leading to improved agent-based models [36], and could also lead to new physics-based models of underwater robots that could be used for improved model-based control of groups.

[Lighthill](#) raised the possibility that the order observed within groups in nature may passively arise due to flow-mediated interactions between group members [37]. Several studies have sought to understand the fluid-mediated dynamics of multiple swimmers interacting with each other [17, 20, 36, 38–45], with nearly all of them being two-dimensional in nature. Ristroph’s work has consistently shown that swimmers in schools passively and stably arrange themselves so that their trajectory has a particular phase offset from incoming vortical

wakes [42–44]. It is important to note that the experiments leading to this conclusion were highly constrained, each model swimmer having only one unconstrained degree of freedom. Additional unconstrained degrees of freedom may qualitatively change the dynamics.

Simplified vortex-dipole models that are still two-dimensional but do not constrain the degrees of freedom have been developed to study the cohesion of groups of swimmers [36, 38–40]. According to these models, purely hydrodynamic interactions are not always enough to maintain cohesive groups; active control on the part of the swimmers is required.

It is unknown how three-dimensional hydrodynamic interactions, as well as the additional degrees of freedom of a three-dimensional world, affect the stability and cohesion of schools. However, it is immediately clear that the three-dimensional dynamics will be different from the two-dimensional dynamics since the velocity field of a three-dimensional swimmer decays with distance r as r^{-3} , while the velocity field of a two-dimensional swimmer decays as r^{-2} . Any potential differences are important since our current understanding of the role of hydrodynamics in collective motion is based on the two-dimensional scenario.

In this work, we take the first step towards understanding the passive group dynamics that develop under three-dimensional hydrodynamic interactions between swimmers. This understanding is enabled by the development of a simple model of a freely moving inertial swimmer that captures the correct leading-order hydrodynamic interactions between swimmers. We consider the elemental interactions between a pair of swimmers. By focusing on their planar dynamics, we are able to conduct a comparative analysis between two-dimensional and three-dimensional swimmers, thereby revealing the significance of three-dimensionality in schooling behavior. Additionally, we make observations on how the geometry of a swimmer affects the dynamics by comparing swimmers that are long and thin to those that are short and fat.

II. MATHEMATICAL MODEL

At the large Reynolds numbers possessed by inertial swimmers, the flow away from their bodies is well described by potential flow. Here, we develop a potential flow model of hydrodynamic interactions between swimmers. First, we describe the flow induced by the motion of one swimmer. Then, we develop a model for the dynamics of multiple swimmers.

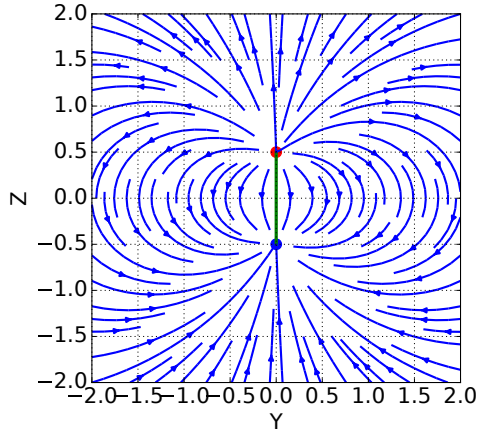


FIG. 1. Streamlines in a plane containing the swimmer. The swimmer is oriented along the z -axis. The source is highlighted in red and the sink in blue.

A. Flow induced by one swimmer

The flow induced by the motion of a body can be expressed in a multipole expansion. For a body of constant volume, the leading-order term is a dipole [46, Ch. 4.7], otherwise called a source doublet [47, Ch. 6.4]. This motivates modeling a swimmer as a source-sink pair of equal strength separated by a fixed distance ℓ , which yields a dipole flow at large distances while also endowing a length scale absent from a doublet. Effectively, our model represents the far field of a swimmer. As will become clear later, the separation between the source and sink unlocks non-trivial rotational dynamics in our model swimmers. The streamlines in a plane containing the source-sink pair are shown in Figure 1. From a physical standpoint, the source represents the fore of a swimmer, which pushes fluid away as the swimmer moves forward. Conversely, the sink represents the rear of a swimmer, where fluid must rush in to fill the void left by the rear as the swimmer moves forward.

To validate the source-sink pair as an effective representation of a swimmer, we compare the flow field generated by our model to that generated by a tuna, as calculated in the simulations of Zhu *et al.* [48]. In their work, Zhu *et al.* employed a three-dimensional panel method to simulate both fish and fish-like robots in an inviscid flow, which agreed reasonably with experimental measurements. The streamlines produced by the source-sink pair are shown in three different planes in Figures 1 and 2. The qualitative agreement with the streamlines of the higher-fidelity tuna simulations is excellent outside of the wake region

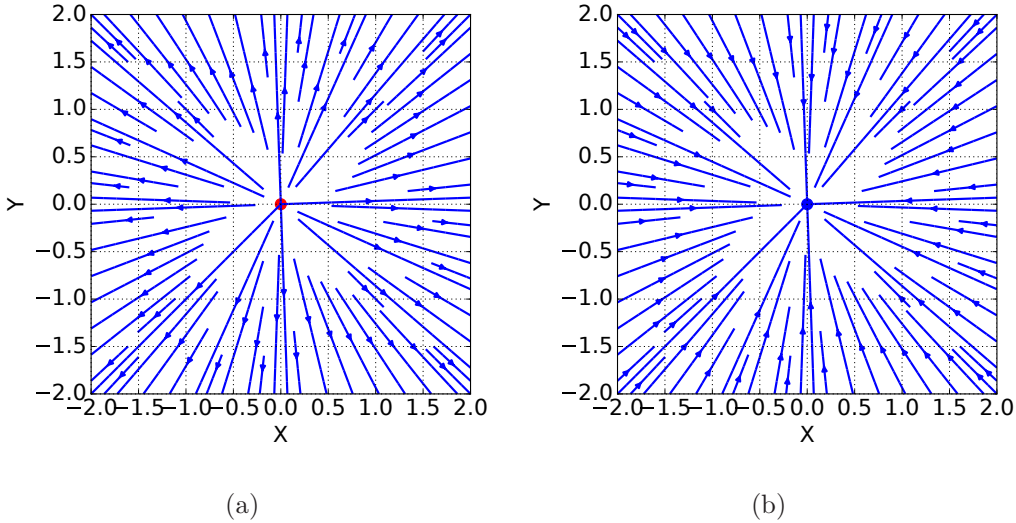


FIG. 2. (a) Cross-sectional view of the streamlines in the plane $z = 0.5$. (b) Cross-sectional view of the streamlines in the plane $z = -0.5$. The swimmer is the same as in Figure 1.

(cf. Figure 5 in [48]). Even very close to the body (within a small fraction of the length of the body) the qualitative agreement is excellent. The streamlines in the wake region differ, which is to be expected since our model does not include vortex shedding. Despite this limitation, our approach should reasonably model the far-field hydrodynamic interactions between swimmers. We return to a discussion of the limitations of the model later.

Alternatively, one could model the swimmer as a thin vortex ring of fixed shape, whose streamlines are shown in Figure 3. Although the flow induced by the vortex ring is quite different from that induced by the source-sink pair close to the singularities, the far-field flows are both dipolar and are therefore representative of what one would expect from a swimmer. In prior two-dimensional work, swimmers have been modeled as counter-rotating pairs of point vortices [36, 38–41], analogous to a thin vortex ring in three dimensions.

We explored modeling a swimmer as a thin three-dimensional vortex ring. In our model, the ring was discretized into a set of evenly spaced material points, induced velocities were evaluated using the Biot-Savart law as described in [49], the cut-off method was employed to de-singularize induced velocity calculations [50, Ch. 11.1], and we developed a numerical procedure to enforce that the shape of the vortex ring not change in time. Besides being more complex and computationally expensive than the source-sink pair model, we believe that the vortex ring model is less representative of typical swimmers for reasons that will be clarified in the ensuing section. Thus, the work described here focuses on the source-sink

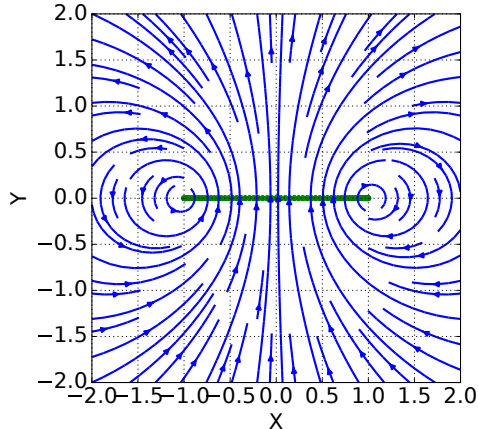


FIG. 3. Streamlines in the plane of rotational symmetry for a vortex ring.

pair model.

B. Dynamics of freely moving swimmers

At a displacement \mathbf{r} away from a source, the velocity induced by it is:

$$\mathbf{u} = \frac{\sigma}{4\pi} \frac{\mathbf{r}}{r^3}, \quad (1)$$

where $\sigma \geq 0$ is the volumetric flow rate, and $r = |\mathbf{r}|$. The velocity induced by a sink is the negative of the above expression.

The strength of the source and sink that comprise the model swimmer clearly should be related to the speed of the swimmer. We take the swimmer's speed U to be equal in magnitude to the velocity that the source (sink) induces on the sink (source), $U = \frac{\sigma}{4\pi\ell^2}$, but opposite in direction in order to be consistent with the physical picture that the source corresponds to the fore of the body and the sink to the rear. An isolated swimmer moves in the direction parallel to its body at a speed U , and we refer to its velocity as the self-propelled velocity.

When more than one swimmer is present, they will mutually affect each other's motions. For each swimmer, we take the velocity of the source to be equal to the sum of the self-propelled velocity and the velocity induced by the sources and sinks of all other swimmers. The velocity of the sink is calculated the same way. In other words, the source and sink are effectively treated as material points. Since swimmers have approximately the same density as the surrounding fluid, treating the velocities of the source and sink in this way is

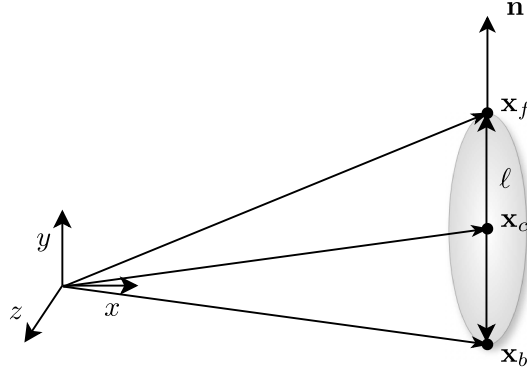


FIG. 4. Representation of a single swimmer.

reasonable. In contrast, this may be a poor approach for flying animals (depending on their size) since they are typically significantly denser than the air they fly in; the relatively high inertia of a flying animal would lead it to respond much more slowly to its surrounding flow.

Left unconstrained, the distance between the source and sink would not remain constant, corresponding to a swimmer whose length changes. To maintain a constant distance between the source and the sink, we adopt the following procedure, which is applied to every swimmer. Let \mathbf{x}_f be the position of the source, \mathbf{x}_b the position of the sink, and \mathbf{x}_c the position of the swimmer's center, so that $\mathbf{x}_c = \frac{1}{2}(\mathbf{x}_f + \mathbf{x}_b)$. The swimmer's configuration is completely specified by the position of its center and its orientation, which is given by a unit vector \mathbf{n} that points from the sink to the source; see Figure 4. We express \mathbf{x}_f and \mathbf{x}_b in terms of \mathbf{x}_c , the swimmer's length ℓ , and the swimmer's orientation:

$$\begin{aligned}\mathbf{x}_f &= \mathbf{x}_c + \frac{1}{2}\ell\mathbf{n}, \\ \mathbf{x}_b &= \mathbf{x}_c - \frac{1}{2}\ell\mathbf{n}.\end{aligned}\tag{2}$$

The velocities of the source and sink are

$$\begin{aligned}\frac{d\mathbf{x}_f}{dt} &= \mathbf{v}_f + \lambda\mathbf{n}, \\ \frac{d\mathbf{x}_b}{dt} &= \mathbf{v}_b - \lambda\mathbf{n},\end{aligned}\tag{3}$$

where \mathbf{v}_f and \mathbf{v}_b respectively correspond to the unconstrained velocities of the source and sink due to the self-propelled velocity and interactions with other swimmers. The additional term $\lambda\mathbf{n}$, in which λ may be thought of as a Lagrange multiplier, corresponds to an attractive/repulsive velocity that ensures that the length of the swimmer remains constant: $\frac{d\ell}{dt} = 0$. Adding this term is equivalent to a force that acts on the source and the sink to

either push them toward each other or pull them apart. Note that this term acts in the direction of \mathbf{n} and does not produce any net translation or rotation of the swimmer.

To find λ , start with $\mathbf{x}_f - \mathbf{x}_b = \ell \mathbf{n}$ and take the time derivative of this equation to arrive at

$$\mathbf{v}_f - \mathbf{v}_b + 2\lambda \mathbf{n} = \frac{d\ell}{dt} \mathbf{n} + \ell \frac{d\mathbf{n}}{dt}. \quad (4)$$

Taking the dot product with \mathbf{n} and recalling that $\frac{d\mathbf{n}}{dt}$ has no component in the direction of \mathbf{n} yields

$$(\mathbf{v}_f - \mathbf{v}_b) \cdot \mathbf{n} + 2\lambda = \frac{d\ell}{dt} = 0 \implies \lambda = -\frac{1}{2}(\mathbf{v}_f - \mathbf{v}_b) \cdot \mathbf{n}. \quad (5)$$

With λ in hand, we can find equations for the evolution of the swimmer's position \mathbf{x}_c and orientation \mathbf{n} . From (3), the swimmer translates according to

$$\frac{d\mathbf{x}_c}{dt} = \frac{1}{2}(\mathbf{v}_f + \mathbf{v}_b), \quad (6)$$

and from (4), its orientation evolves according to

$$\frac{d\mathbf{n}}{dt} = \frac{1}{\ell}(\mathbf{v}_f - \mathbf{v}_b + 2\lambda \mathbf{n}) = \frac{1}{\ell} \{ \mathbf{v}_f - \mathbf{v}_b - [(\mathbf{v}_f - \mathbf{v}_b) \cdot \mathbf{n}] \mathbf{n} \}. \quad (7)$$

The swimmer translates at the sum of the self-propelled velocity and the average of the induced velocities at its source and sink due to other swimmers. Thus, the swimmer's body acts to spatially filter the velocity field induced by all other swimmers.

The orientation dynamics are rather interesting. Remark that the swimmer can rotate despite the flow being irrotational. This is possible because of the finite length of the swimmer and the non-zero rate of strain in the flow. In (7), the term inside of the braces is the component of $\mathbf{v}_f - \mathbf{v}_b$ perpendicular to \mathbf{n} , i.e., the component in the plane normal to the swimmer's body. The orientation dynamics are thus given by the gradient along the unit normal of the component of the velocity in the plane normal to the swimmer's body. In other words, the swimmer samples the gradient of the crossflow along its body, leading to rotation. A schematic explanation is illustrated in Figure 5. This is how a short, inextensible material line would deform in a flow. For a swimmer modeled as a thin vortex ring, it would sample the gradient of the body-parallel velocity in the plane of the vortex ring (i.e., the gradient *across* the swimmer's body rather than along it), which leads to qualitatively different dynamics. The rotational dynamics are illustrated in Figure 6, and should be contrasted with those of the source-sink pair in Figure 5. For swimmers that are

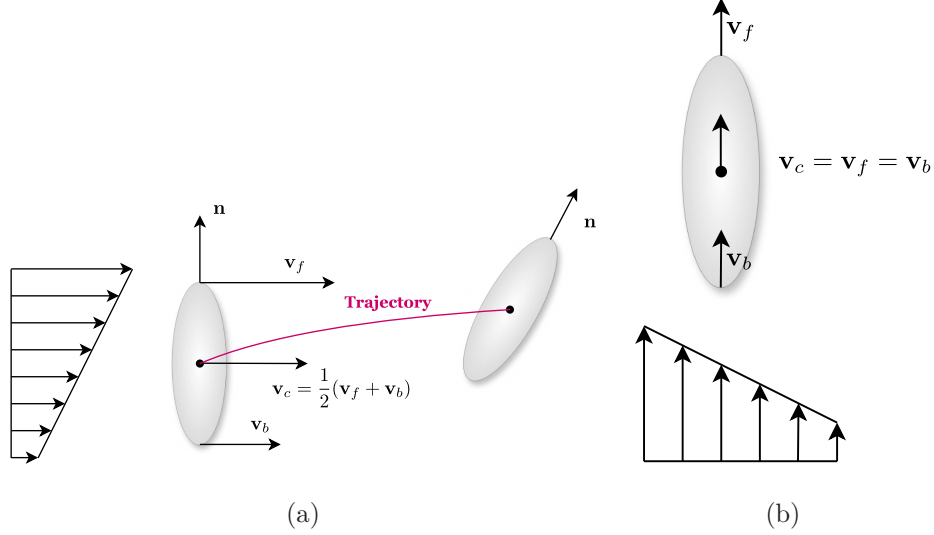


FIG. 5. (a) A gradient along the body of the crossflow results in rotation. (b) A gradient across the body of the body-parallel velocity does not result in rotation.

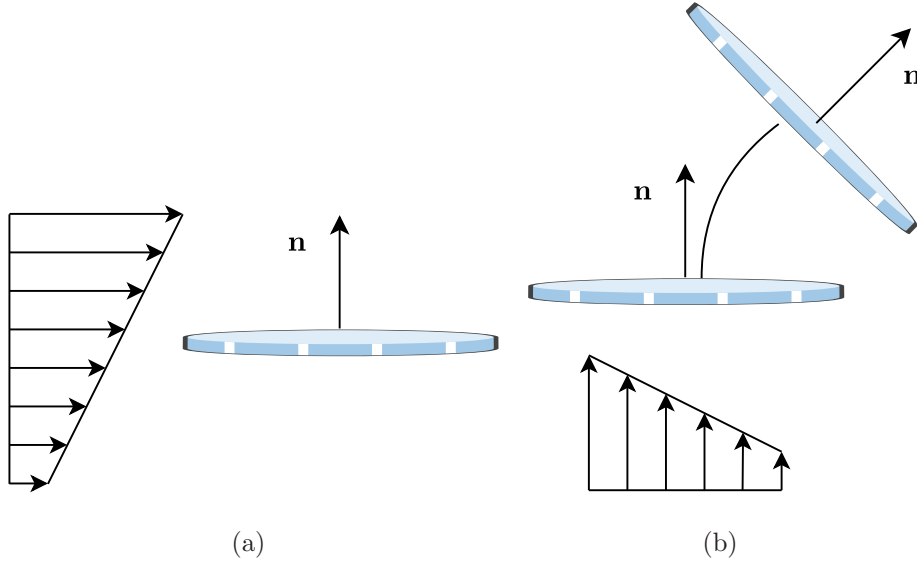


FIG. 6. (a) A gradient along the body of the crossflow does not result in rotation. (b) A gradient across the body of the body-parallel velocity results in rotation.

long and thin, the source-sink pair model is reasonable since the orientation dynamics of such swimmers would be dominated by the crossflow velocity gradient along the length of their bodies. Conversely, the orientation dynamics of short and fat swimmers would be dominated by the velocity gradient across their bodies, making the vortex ring model appropriate in that case. Since most swimmers are long and thin, we use the source-sink pair model.

A dynamical system is formed by concatenating the position and unit normal of each

swimmer into one state vector and evolving it forward in time according to (6) and (7). The dynamics are nonlinear, so we numerically evolve the system forward in time using the fourth-order Runge-Kutta method. At each step, we re-normalize the unit normal of every swimmer to have unit length since this is not maintained by the Runge-Kutta method.

The preceding discussion is unchanged for two-dimensional swimmers, except that the velocity induced by a source in (1) is $\mathbf{u} = \frac{\sigma}{2\pi} \frac{\mathbf{r}}{r^2}$, where σ is the volumetric flow rate per unit depth in two dimensions. In this case, the self-propelled velocity is $U = \frac{\sigma}{2\pi\ell}$.

III. PLANAR DYNAMICS OF A PAIR

We present numerical examples of the three-dimensional dynamic interactions between a pair of identical swimmers. Such pairwise interactions can be thought of as the elemental interactions in a large school. To facilitate comparison with two-dimensional models, we consider planar dynamics, where the swimmers' bodies are co-planar initially and, therefore, for all time. This also allows us to fully characterize the phase space. In what follows, lengths have been non-dimensionalized by the swimmer's length ℓ and velocities have been non-dimensionalized by the self-propelled speed U .

A. Symmetry reduction

With two swimmers, the dimension of the state space is 12, with six variables for each swimmer (three for the position of its center, and three for the unit normal describing its orientation). For the planar motion of two swimmers, however, leveraging symmetry allows us to describe the motion of the pair using only three variables. Specifically, due to a translational symmetry, only the separation between the swimmers' centers (rather than their absolute positions) affects the dynamics. Similarly, a rotational symmetry makes it so that only the relative angle between the swimmers (rather than their absolute orientations) affects the dynamics. Without loss of generality, we place the swimmers in the x - y plane, with one swimmer initially oriented in the positive y -direction, separated from each other by $(\Delta x, \Delta y)$, and with a relative angle $\Delta\theta$ between them, as in Figure 7. In this smaller three-dimensional symmetry-reduced phase space, we can fully characterize the possible dynamics.

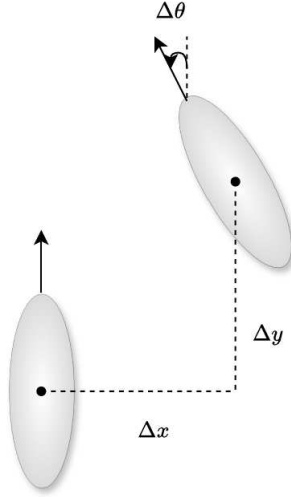


FIG. 7. Symmetry-reduced configuration of a co-planar pair of swimmers.

B. Three-dimensional model

Several qualitatively different sets of dynamics are possible, some simple and expected, others complex and unexpected. The simplest dynamics occur when the swimmers are co-linear ($\Delta x = 0$ and $\Delta\theta \in \{0, \pi\}$). In this case, the swimmers remain co-linear for all time. When the swimmers have the same initial orientation ($\Delta\theta = 0$) and do not intersect ($|\Delta y| > 1$), they move at equal steady speeds, causing their separation Δy to remain constant, no matter its value. Their speed depends on their separation as $v = 1 + \frac{2|\Delta y|}{(\Delta y^2 - 1)^2}$. The speed increases monotonically as the swimmers are positioned closer to each other, reflecting a drafting phenomenon. The speed diverges as $\frac{1}{2(|\Delta y| - 1)^2}$ as $|\Delta y| \rightarrow 1^+$, and approaches the self-propelled speed as $\frac{2}{|\Delta y|^3}$ as $|\Delta y| \rightarrow \infty$, as shown in Figure 8. The divergence in speed when the swimmers are very close is non-physical; we must keep in mind that we model the far-field hydrodynamic interactions, which may poorly reflect reality when the swimmers are very close. Since the separation remains constant, such in-line motion forms a locus of relative equilibria.

When the swimmers are co-linear but have opposite orientations ($\Delta\theta = \pi$), they can either face each other ($\Delta y > 1$) or face away from each other ($\Delta y < -1$). When they face each other, they approach each other at a speed $\frac{d\Delta y}{dt} = -2 + \frac{4\Delta y}{(\Delta y^2 - 1)^2}$. Note that there is a stable equilibrium at $\Delta y \approx 1.684$ where the swimmers directly face each other and do not move. At smaller separations the swimmers push each other away, while at larger

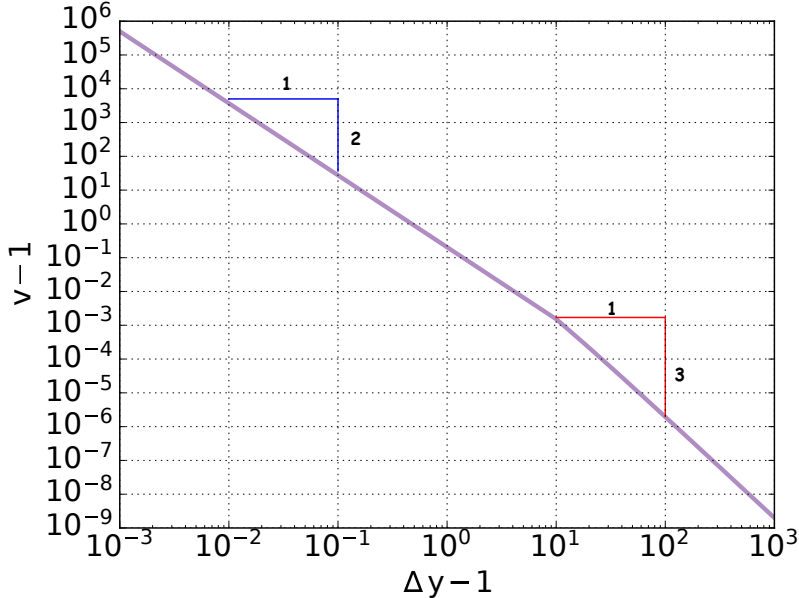


FIG. 8. Swimmers' speed as a function of their separation for a co-linear configuration for the three-dimensional model.

separations the swimmers approach this equilibrium. When the swimmers face away from each other, they continually separate at a speed $\frac{d\Delta y}{dt} = 2 - \frac{4\Delta y}{(\Delta y^2 - 1)^2}$, quickly approaching their self-propelled speeds as $|\Delta y|^{-3}$.

For initial configurations where the swimmers are not co-linear, we observe several interesting behaviors. To start, we consider the case when the swimmers have the same orientation ($\Delta\theta = 0$). When the separation between the swimmers is small, they may collide into each other. Such collisions are non-physical—at least for the manner in which they occur under our model, where the swimmers turn away from each other before their rears suck each other in (Figure 9(a)). At larger separations, the swimmers can diverge from each other (Figure 9(b)), they can become locked in a simple braid-like motion that is a relative periodic orbit (Figure 9(c)), or they can become locked in a complex braid-like motion that is also a relative periodic orbit (Figure 9(d)). Complex braid-like motions are those where the path of a swimmer intersects itself. For the relative periodic orbits, the relevant symmetry is the translational symmetry. The latter two types of motions correspond to a cohesive pair of swimmers.

The possible behaviors for $\Delta\theta = 0$ are summarized in the phase diagram in Figure 10, which shows what behaviors are achieved for given initial configurations. There is a clear

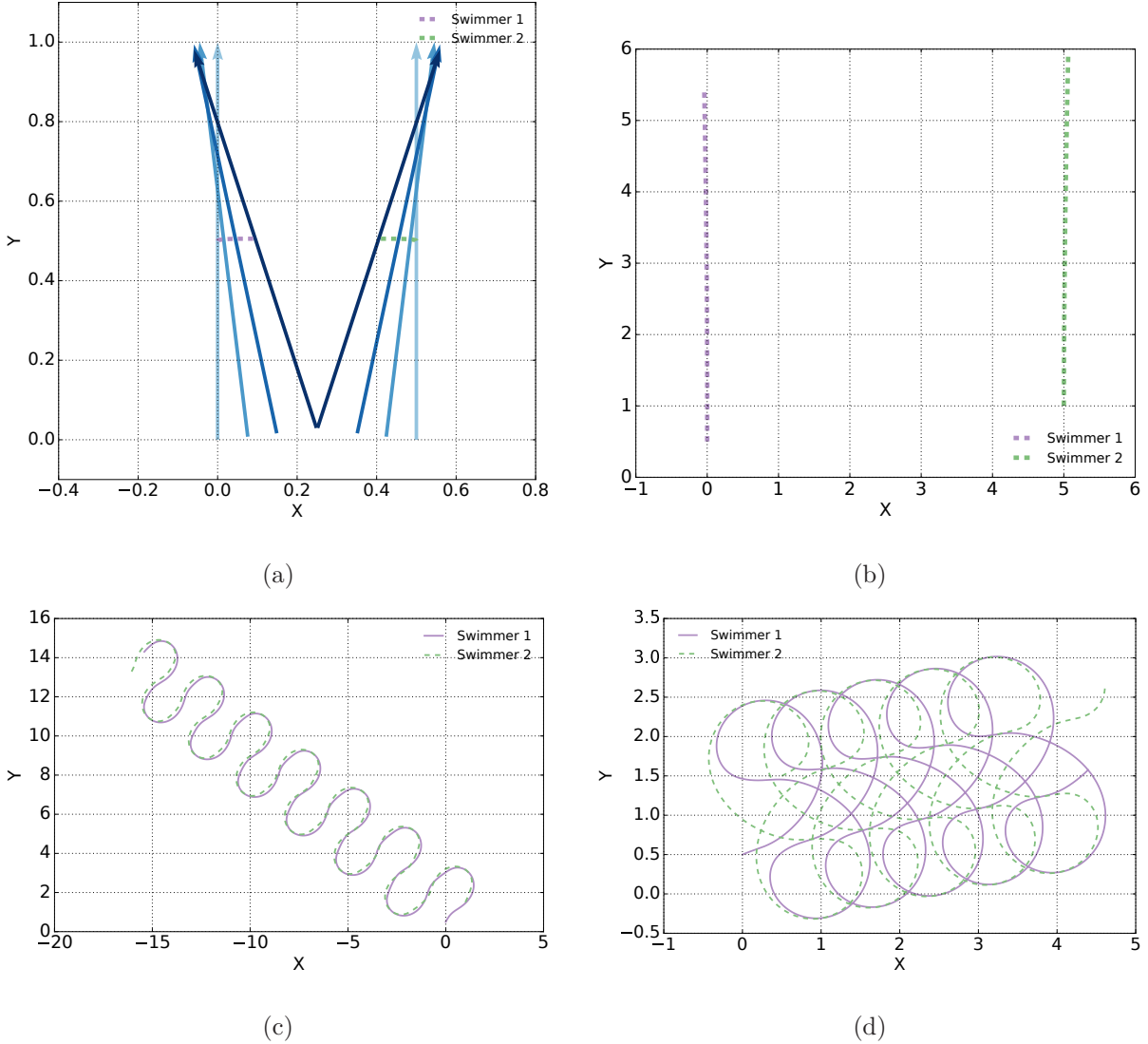


FIG. 9. Planar trajectories of two swimmers for different initial conditions with $\Delta\theta = 0$. (a) $\Delta\theta = 0$, $\Delta x = 0.5$, $\Delta y = 0$. In (a), the two swimmer's bodies are represented by arrows whose colors represent time (darker is a later time). (b) $\Delta\theta = 0$, $\Delta x = 5$, $\Delta y = 0.5$. (c) $\Delta\theta = 0$, $\Delta x = 1$, $\Delta y = 1$. (d) $\Delta\theta = 0$, $\Delta x = 0.5$, $\Delta y = 1$.

division between configurations that lead to divergent motions and those that lead to cohesive motions. The boundary between the two is especially of interest to us because we are ultimately interested in whether cohesive groups can be formed by passive hydrodynamic interactions alone. The boundary separates configurations that lead to cohesive groups from those that do not.

To locate the boundary separating cohesive initial configurations from divergent configurations, we use the fact that a configuration on the boundary is a relative equilibrium of

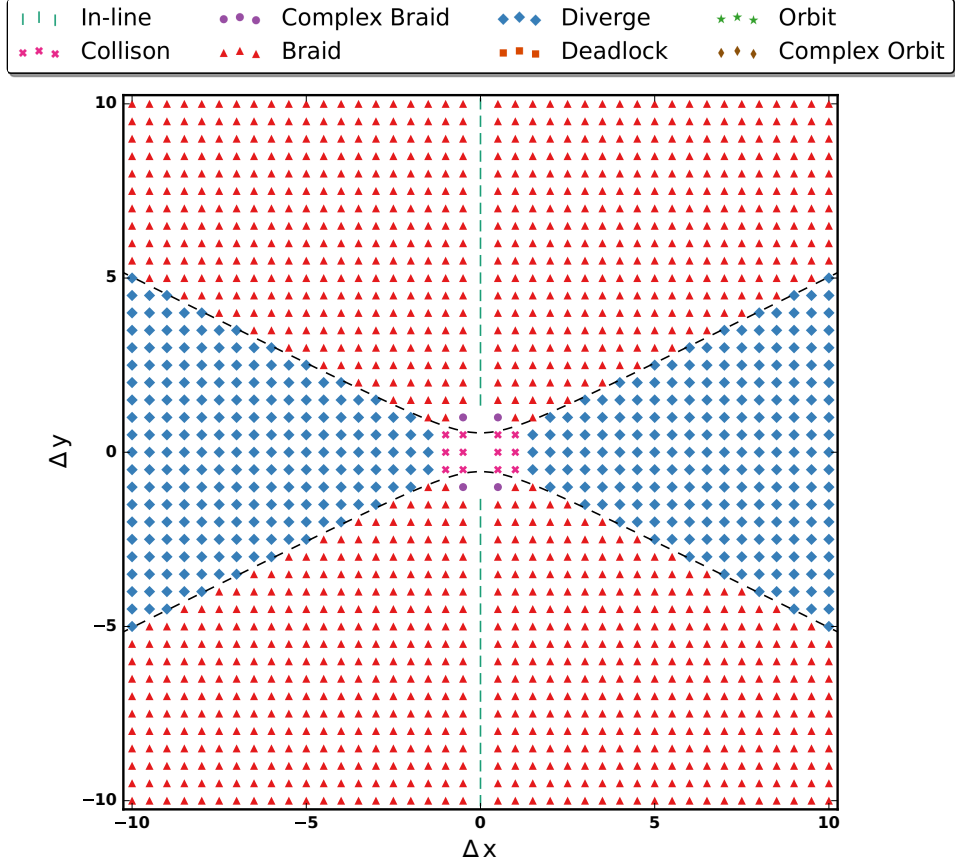


FIG. 10. Phase diagram for $\Delta\theta = 0$ for three-dimensional swimmers.

the dynamical system. Moreover, in a boundary configuration, the swimmers do not rotate. Since, without loss of generality, the swimmers' unit normals both point in the positive y -direction in their initial configuration, boundary configurations must satisfy $\frac{d\mathbf{n}}{dt} \cdot \mathbf{e}_1 = 0$, where \mathbf{e}_1 is the unit vector in the positive x -direction. Applying this condition to one of the swimmers yields an implicit equation for the boundary,

$$\frac{2\Delta x}{(\Delta x^2 + \Delta y^2)^{3/2}} - \frac{\Delta x}{[\Delta x^2 + (\Delta y - 1)^2]^{3/2}} - \frac{\Delta x}{[\Delta x^2 + (\Delta y + 1)^2]^{3/2}} = 0, \quad (8)$$

which we solve numerically using a root-finding algorithm. At large separations, the boundary is given by $|\Delta y| \approx \frac{1}{2}|\Delta x|$. The boundary is drawn in the phase diagram in Figure 10. Note the mirror symmetry across both axes.

For initial configurations with $\Delta\theta \neq 0$, in addition to the classes of motion observed when $\Delta\theta = 0$, we also observe orbital motions (Figure 11(a)) and complex orbital motions (Figure 11(b)). Complex orbital motions are those for which $\frac{d\theta}{dt}$ changes sign for each swimmer,

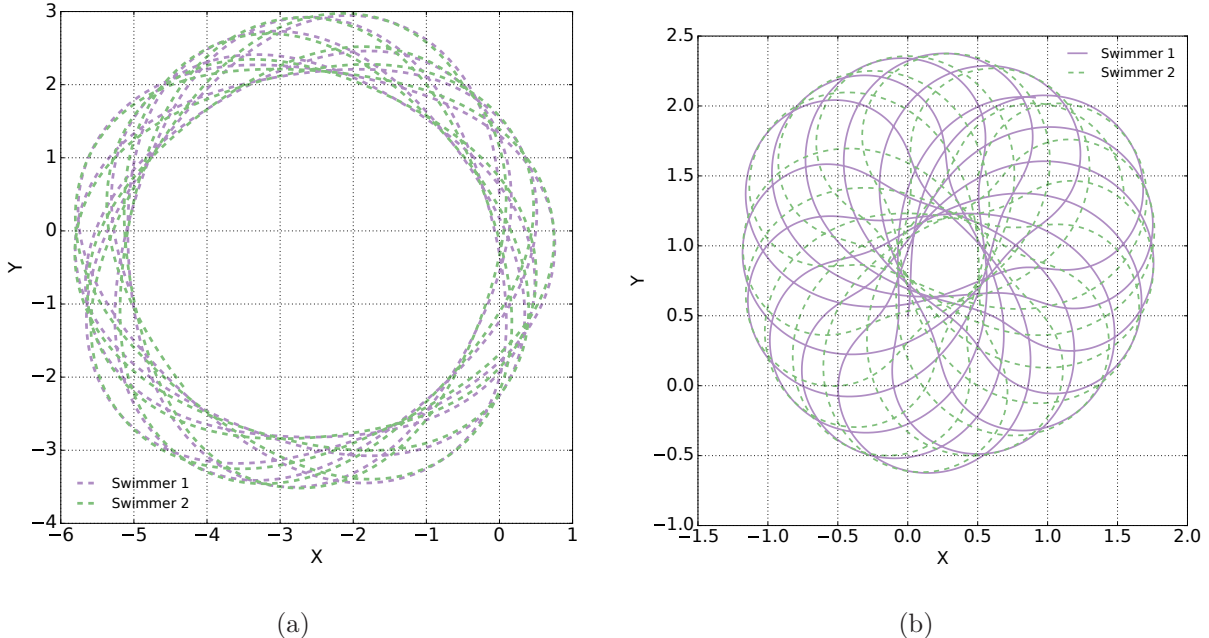


FIG. 11. Planar trajectories of a pair of swimmers for different initial conditions with $\Delta\theta \neq 0$. (a) $\Delta\theta = \frac{\pi}{4}$, $\Delta x = -0.5$, $\Delta y = 1.5$. (b) $\Delta\theta = \frac{\pi}{3}$, $\Delta x = 0.5$, $\Delta y = 1.0$.

where θ gives the orientation of a swimmer. Both of these classes of motion correspond to relative periodic orbits, where the relevant symmetry is the rotational symmetry, not the translational symmetry as for the braid-like motions. Without symmetry reduction, the dynamics are quasiperiodic. Notably, swimmers undergoing these motions have no net displacement.

The possible behaviors for $\Delta\theta \neq 0$ are summarized in the phase diagrams in Appendix A, which show what behaviors are achieved for given initial configurations. In contrast to when $\Delta\theta = 0$, the set of configurations leading to a cohesive group is compact and decreases in size as $|\Delta\theta|$ increases. In other words, misalignment of the swimmers leads them to diverge from each other.

We can gain some additional insight from the full three-dimensional symmetry-reduced phase diagram. In Figure 12(a), we show the volume of configurations that lead to a cohesive group. The central column mostly consists of configurations causing the swimmers to non-physically collide. The volume consists of a continuum of relative periodic orbits, some of which are included for illustration in Figure 12(b). We have also plotted the boundary separating cohesive configurations from divergent ones for $\Delta\theta = 0$. Recall that the boundary consists of relative equilibria. The bottom and top surfaces of the volume meet

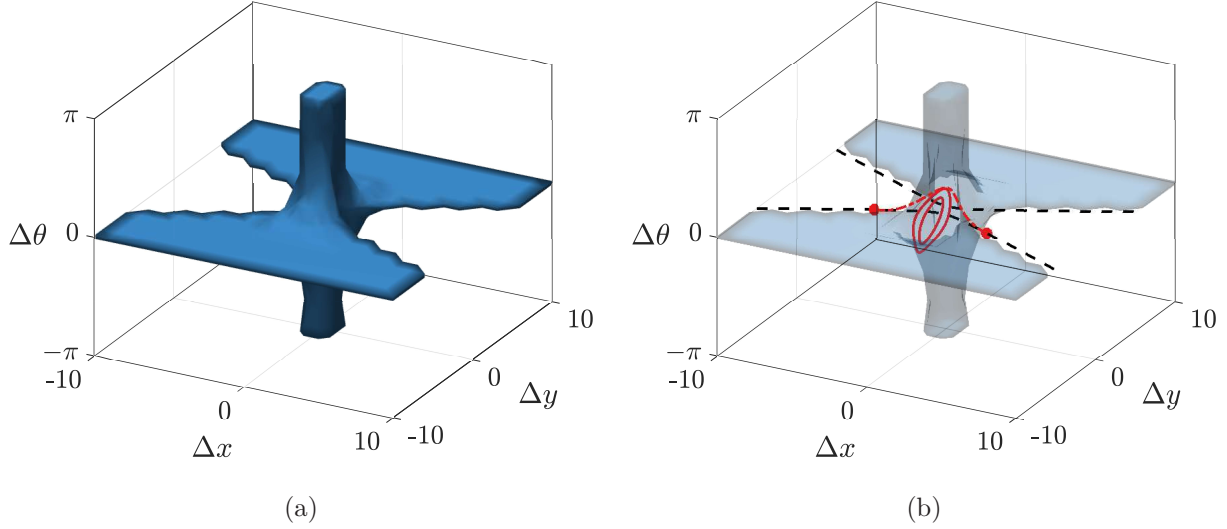


FIG. 12. (a) Configurations in the symmetry-reduced phase space that lead to a cohesive group. (b) Dynamical features of importance: relative periodic orbits (solid red); locus of relative equilibria (dashed black); and relative heteroclinic orbit (dash-dotted red) connecting two relative equilibria (red points).

at this boundary. These bottom and top surfaces, therefore, contain a continuum of heteroclinic connections in the symmetry-reduced phase space, an example of which is shown in Figure 12(b). Each relative heteroclinic connection corresponds to a transition from one steadily moving configuration to another.

C. Two-dimensional model

The phase diagrams for the two-dimensional swimmers are shown in Appendix B. There are no significant qualitative differences between them and the phase diagrams for three-dimensional swimmers. The observations we have made regarding group cohesion for three-dimensional swimmers transfer over to two-dimensional swimmers.

There are some quantitative differences worth noting. When the swimmers are co-linear, have the same initial orientation ($\Delta\theta = 0$), and do not intersect ($|\Delta y| > 1$), they move at equal steady speeds that depend on their separation as $v = 1 + \frac{1}{\Delta y^2 - 1}$. The speed increases monotonically as the swimmers are positioned closer to each other. The speed diverges as $\frac{1}{2(|\Delta y| - 1)}$ as $|\Delta y| \rightarrow 1^+$, and approaches the self-propelled speed as $\frac{1}{\Delta y^2}$ as $|\Delta y| \rightarrow \infty$, as shown in Figure 13. The speed is greater than in the three-dimensional model when

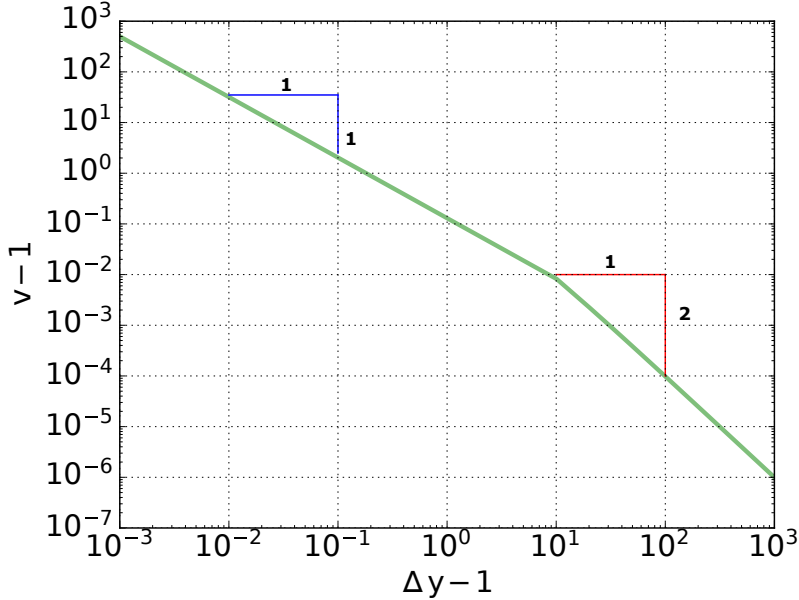


FIG. 13. Swimmers' speed as a function of their separation for a co-linear configuration for the two-dimensional model.

$|\Delta y| > 1 + \sqrt{2}$, but is less for closer separations. When the swimmers are co-linear but have opposite orientations ($\Delta\theta = \pi$), they can either face each other ($\Delta y > 1$) or face away from each other ($\Delta y < -1$). When they face each other, they approach each other at a speed $\frac{d\Delta y}{dt} = -2 + \frac{2}{\Delta y^2 - 1}$. There is a stable equilibrium at $\Delta y = \sqrt{2}$, which is closer than in the three-dimensional model. When the swimmers face away from each other, they continually separate at a speed $\frac{d\Delta y}{dt} = 2 - \frac{2}{\Delta y^2 - 1}$, quickly approaching their self-propelled speeds as $|\Delta y|^{-2}$.

The two-dimensional model also shows a clear boundary in phase space separating cohesive and divergent configurations when $\Delta\theta = 0$, corresponding to a locus of relative equilibria. The phase diagram and boundary are shown in Figure 14. The boundary satisfies

$$\frac{2\Delta x}{\Delta x^2 + \Delta y^2} - \frac{\Delta x}{\Delta x^2 + (\Delta y - 1)^2} - \frac{\Delta x}{\Delta x^2 + (\Delta y + 1)^2} = 0. \quad (9)$$

At large separations, the boundary is given by $|\Delta y| \approx \frac{1}{\sqrt{3}}|\Delta x|$. The set of cohesive configurations is larger for the three-dimensional model.

Although the two-dimensional swimmers largely have the same behavior as the three-dimensional swimmers, we emphasize that we have only compared the planar dynamics since two-dimensional swimmers are limited to planar dynamics. The three-dimensional

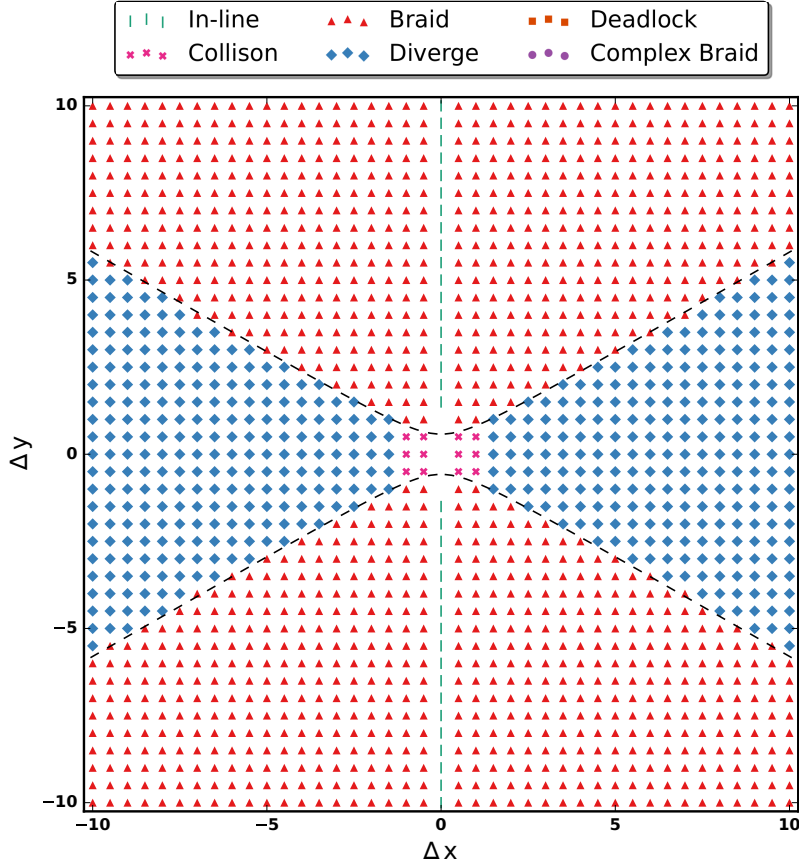


FIG. 14. Phase diagram for $\Delta\theta = 0$ for two-dimensional swimmers.

model we have developed allows for non-planar dynamics, thereby enabling the study of the dynamics of three-dimensional schools.

D. Geometric effects

Finally, we briefly study the effects of geometry by comparing long and thin swimmers (source-sink pairs) to short and fat swimmers (vortex ring model). The phase diagram for the planar dynamics of two initially aligned ($\Delta\theta = 0$) vortex-ring swimmers is shown in Figure 15. The region where the vortex rings overlap is excluded. We observe four types of motions: in-line motion, divergence, collision, and oscillatory motion. Oscillatory motion is qualitatively similar to the braid-like motion in Figure 9, except that the paths of the swimmers do not intersect, instead following an alternating pattern of convergence and divergence. Although the types of motions are similar to what is observed for the

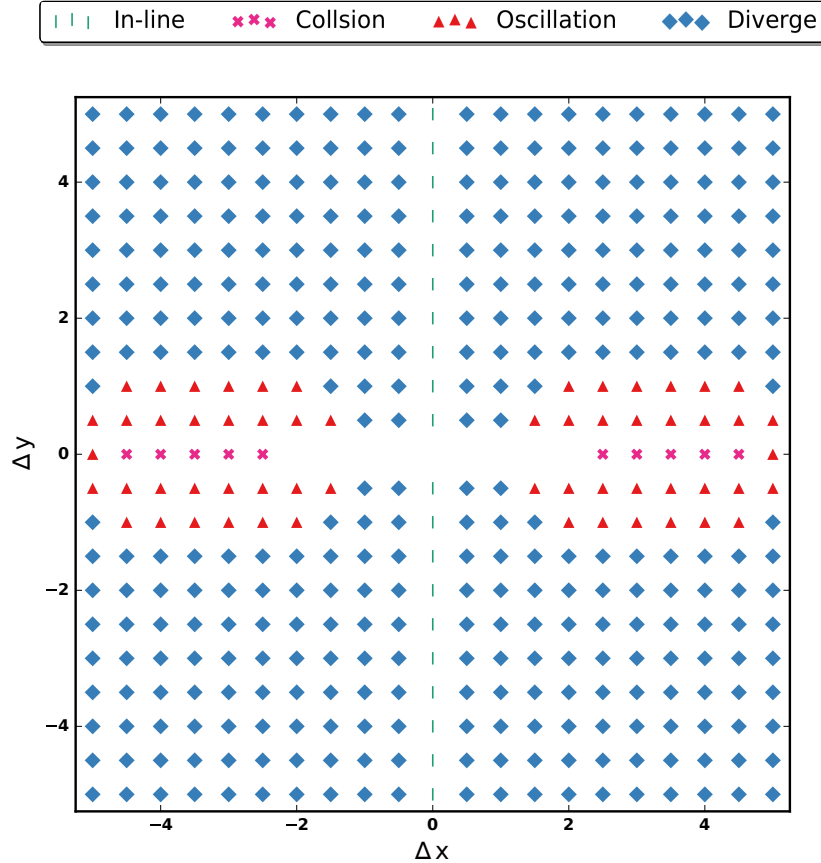


FIG. 15. Phase diagram for $\Delta\theta = 0$ for three-dimensional swimmers modeled as thin vortex rings.

source-sink model, the phase diagram differs substantially. First, the set of configurations leading to a cohesive group is much smaller than for the source-sink model. Second, cohesive configurations have small vertical separations, while for the source-sink model they had large vertical separations. Third, the vortex rings collide only when $\Delta y = 0$; when they collide, they do so by turning head-on towards each other. These qualitative differences in the dynamics of short and fat swimmers compared to long and thin swimmers can be rationalized by appealing to how these two types of swimmers sample the velocity gradient, as was explained in Figures 5 and 6. Interestingly, the dynamics we observe in our vortex ring model are qualitatively similar to the dynamics observed for toroidal swimmers in Stokes flow [51], despite being at opposite ends of the Reynolds number spectrum.

IV. CONCLUSION

The collective motion of inertial swimming animals confers several benefits, but they can be realized only if a cohesive group can be maintained. Group cohesion depends on the dynamics of freely moving swimmers, in which the passive hydrodynamic interactions between individuals play a strong role. This naturally leads one to ask whether a cohesive group can form passively through hydrodynamic interactions alone.

To understand the passive group dynamics, we developed a simplified model of the three-dimensional hydrodynamic interactions between freely moving inertial swimmers. Our model is based on the leading-order term of the multipole expansion of the velocity field, and is therefore a far-field model. Nevertheless, the model accurately captures the flow created by commonly found long and thin swimmers, at least qualitatively. Of note is the very low computational cost of our model.

Since the passive dynamics of swimmers with three-dimensional hydrodynamic interactions had not been studied before, we first sought to understand the role of three-dimensionality. This was accomplished by studying the planar dynamics of a pair of swimmers and comparing them to the dynamics of a pair of swimmers with two-dimensional hydrodynamic interactions. We observed many interesting dynamics: braid-like motions, orbiting motions, divergent motions, and others, which were thoroughly characterized by phase diagrams. In state space, we observed relative equilibria, relative periodic orbits, quasiperiodic orbits, and relative heteroclinic connections. Most importantly, we found that certain configurations of the swimmers led to a cohesive group, and that misalignment of the swimmers led them to diverge from each other.

The two-dimensional swimmers largely have the same planar dynamics as the three-dimensional swimmers. However, our three-dimensional model enables the study of non-planar dynamics and three-dimensional schools, which we will pursue in future work.

We also studied the effects of geometry, finding that long and thin swimmers have qualitatively different dynamics than short and fat swimmers. The differences are due to the geometry affecting how the velocity gradient is sampled: the rotational dynamics of long and thin swimmers are dominated by the gradient along their bodies of the crossflow, while for short and fat swimmers they are dominated by the gradient across their bodies of the body-parallel flow.

In principle, models that make no simplifications can be developed. This would amount to direct numerical simulations of schools of freely moving swimmers. The largest such three-dimensional simulation that we are aware of is a recent simulation of a school of 350 swimmers [52]. This single simulation required parallel computing with adaptive meshing, and significant compute time on a large computing cluster. With a Reynolds number of 4000 (using the flapping speed as the velocity scale), the simulated swimmers correspond to a typical natural swimmer of roughly 1 cm in length [53]. This simulation is a feat of scientific computing, but it also underscores that, as a community, we are incredibly far from having the ability to conduct full-fidelity simulations of large groups of large swimmers. The model we have developed in the present work allows us to explore this very interesting space of large groups of inertia-dominated swimmers (at the cost of truncated physics). Ultimately, we aim to provide insights into suspensions of inertial swimmers, as has been done in the viscosity-dominated limit [54].

-
- [1] T. Vicsek and A. Zafeiris, Collective motion, *Physics Reports* **517**, 71 (2012).
 - [2] J. Gautrais, C. Jost, and G. Theraulaz, Key behavioural factors in a self-organised fish school model, *Annales Zoologici Fennici* **45**, 415 (2008).
 - [3] P. F. Major, Predator-prey interactions in two schooling fishes, *caranx ignobilis* and *stolephorus purpureus*, *Animal Behaviour* **26**, 760 (1978).
 - [4] E. Shaw, Schooling fishes, *American Scientist* **66**, 166 (1978).
 - [5] L. Landeau and J. Terborgh, Oddity and the ‘confusion effect’ in predation, *Animal Behaviour* **34**, 1372 (1986).
 - [6] T. J. Pitcher, A. E. Magurran, and I. J. Winfield, Fish in larger shoals find food faster, *Behavioral Ecology and Sociobiology* **10**, 149 (1982).
 - [7] R. S. K. Barnes and R. N. Hughes, *An introduction to marine ecology* (John Wiley & Sons, 1999).
 - [8] D. Weihs, Hydromechanics of fish schooling, *Nature* **241**, 290 (1973).
 - [9] M. Brambilla, E. Ferrante, M. Birattari, and M. Dorigo, Swarm robotics: a review from the swarm engineering perspective, *Swarm Intelligence* **7**, 1 (2013).
 - [10] M. Rubenstein, A. Cornejo, and R. Nagpal, Programmable self-assembly in a thousand-robot

- swarm, *Science* **345**, 795 (2014).
- [11] M. Dorigo, G. Theraulaz, and V. Trianni, Reflections on the future of swarm robotics, *Science Robotics* **5**, eabe4385 (2020).
- [12] D. M. Gordon, *Ant encounters: interaction networks and colony behavior* (Princeton University Press, 2010).
- [13] L. Li, M. Nagy, J. M. Graving, J. Bak-Coleman, G. Xie, and I. D. Couzin, Vortex phase matching as a strategy for schooling in robots and in fish, *Nature Communications* **11**, 5408 (2020).
- [14] S. Verma, G. Novati, and P. Koumoutsakos, Efficient collective swimming by harnessing vortices through deep reinforcement learning, *Proceedings of the National Academy of Sciences* **115**, 5849 (2018).
- [15] I. Ashraf, H. Bradshaw, T.-T. Ha, J. Halloy, R. Godoy-Diana, and B. Thiria, Simple phalanx pattern leads to energy saving in cohesive fish schooling, *Proceedings of the National Academy of Sciences* **114**, 9599 (2017).
- [16] G. Novati, S. Verma, D. Alexeev, D. Rossinelli, W. M. Van Rees, and P. Koumoutsakos, Synchronisation through learning for two self-propelled swimmers, *Bioinspiration & Biomimetics* **12**, 036001 (2017).
- [17] A. U. Oza, L. Ristroph, and M. J. Shelley, Lattices of hydrodynamically interacting flapping swimmers, *Physical Review X* **9**, 041024 (2019).
- [18] S. Alben, Collective locomotion of two-dimensional lattices of flapping plates. part 1. numerical method, single-plate case and lattice input power, *Journal of Fluid Mechanics* **915**, A20 (2021).
- [19] S. Alben, Collective locomotion of two-dimensional lattices of flapping plates. part 2. lattice flows and propulsive efficiency, *Journal of Fluid Mechanics* **915**, A21 (2021).
- [20] J. W. Newbolt, J. Zhang, and L. Ristroph, Lateral flow interactions enhance speed and stabilize formations of flapping swimmers, *Physical Review Fluids* **7**, L061101 (2022).
- [21] M. Kurt and K. W. Moored, Flow interactions of two-and three-dimensional networked bio-inspired control elements in an in-line arrangement, *Bioinspiration & Biomimetics* **13**, 045002 (2018).
- [22] B. M. Boschitsch, P. A. Dewey, and A. J. Smits, Propulsive performance of unsteady tandem hydrofoils in an in-line configuration, *Physics of Fluids* **26** (2014).
- [23] P. A. Dewey, D. B. Quinn, B. M. Boschitsch, and A. J. Smits, Propulsive performance of

- unsteady tandem hydrofoils in a side-by-side configuration, *Physics of Fluids* **26** (2014).
- [24] Y. Pan and H. Dong, Computational analysis of hydrodynamic interactions in a high-density fish school, *Physics of Fluids* **32** (2020).
- [25] L. E. Muscutt, G. D. Weymouth, and B. Ganapathisubramani, Performance augmentation mechanism of in-line tandem flapping foils, *Journal of Fluid Mechanics* **827**, 484 (2017).
- [26] J.-H. Seo and R. Mittal, Improved swimming performance in schooling fish via leading-edge vortex enhancement, *Bioinspiration & Biomimetics* **17**, 066020 (2022).
- [27] Y. Pan and H. Dong, Effects of phase difference on hydrodynamic interactions and wake patterns in high-density fish schools, *Physics of Fluids* **34** (2022).
- [28] M. Saadat, F. Berlinger, A. Sheshmani, R. Nagpal, G. V. Lauder, and H. Haj-Hariri, Hydrodynamic advantages of in-line schooling, *Bioinspiration & Biomimetics* **16**, 046002 (2021).
- [29] I. D. Couzin and J. Krause, Self-organization and collective behavior in vertebrates, *Advances in the Study of Behavior* **32**, 10 (2003).
- [30] I. D. Couzin, J. Krause, N. R. Franks, and S. A. Levin, Effective leadership and decision-making in animal groups on the move, *Nature* **433**, 513 (2005).
- [31] C. M. Breder, Equations descriptive of fish schools and other animal aggregations, *Ecology* **35**, 361 (1954).
- [32] I. Aoki, A simulation study on the schooling mechanism in fish, [NIPPON SUISAN GAKKAISHI](#) **48**, 1081 (1982).
- [33] C. W. Reynolds, Flocks, herds and schools: A distributed behavioral model, in *Proceedings of the 14th annual conference on Computer graphics and interactive techniques* (1987) pp. 25–34.
- [34] I. D. Couzin, J. Krause, R. James, G. D. Ruxton, and N. R. Franks, Collective memory and spatial sorting in animal groups, *Journal of Theoretical Biology* **218**, 1 (2002).
- [35] H. Ko, G. Lauder, and R. Nagpal, The role of hydrodynamics in collective motions of fish schools and bioinspired underwater robots, *Journal of the Royal Society Interface* **20**, 20230357 (2023).
- [36] A. Filella, F. Nadal, C. Sire, E. Kanso, and C. Eloy, Model of collective fish behavior with hydrodynamic interactions, *Physical Review Letters* **120**, 198101 (2018).
- [37] J. Lighthill, *Mathematical biofluidynamics* (SIAM, 1975).
- [38] A. A. Tchieu, E. Kanso, and P. K. Newton, The finite-dipole dynamical system, *Proceedings of the Royal Society A: Mathematical, Physical and Engineering Sciences* **468**, 3006 (2012).

- [39] E. Kanso and A. C. H. Tsang, Dipole models of self-propelled bodies, *Fluid Dynamics Research* **46**, 061407 (2014).
- [40] M. Gazzola, A. A. Tchieu, D. Alexeev, A. De Brauer, and P. Koumoutsakos, Learning to school in the presence of hydrodynamic interactions, *Journal of Fluid Mechanics* **789**, 726 (2016).
- [41] M. Porfiri, P. Zhang, and S. D. Peterson, Hydrodynamic model of fish orientation in a channel flow, *eLife* **11**, e75225 (2022).
- [42] A. D. Becker, H. Masoud, J. W. Newbolt, M. Shelley, and L. Ristroph, Hydrodynamic schooling of flapping swimmers, *Nature Communications* **6**, 8514 (2015).
- [43] S. Ramananarivo, F. Fang, A. Oza, J. Zhang, and L. Ristroph, Flow interactions lead to orderly formations of flapping wings in forward flight, *Physical Review Fluids* **1**, 071201 (2016).
- [44] J. W. Newbolt, J. Zhang, and L. Ristroph, Flow interactions between uncoordinated flapping swimmers give rise to group cohesion, *Proceedings of the National Academy of Sciences* **116**, 2419 (2019).
- [45] M. Gazzola, B. Hejazialhosseini, and P. Koumoutsakos, Reinforcement learning and wavelet adapted vortex methods for simulations of self-propelled swimmers, *SIAM Journal on Scientific Computing* **36**, B622 (2014).
- [46] J. D. Eldredge, *Mathematical Modeling of Unsteady Inviscid Flows*, Vol. 50 (Springer, 2019).
- [47] G. K. Batchelor, *An Introduction to Fluid Dynamics* (Cambridge University Press, 2000).
- [48] Q. Zhu, M. Wolfgang, D. Yue, and M. Triantafyllou, Three-dimensional flow structures and vorticity control in fish-like swimming, *Journal of Fluid Mechanics* **468**, 1 (2002).
- [49] Y. Kimura and H. Moffatt, Scaling properties towards vortex reconnection under biot–savart evolution, *Fluid Dynamics Research* **50**, 011409 (2017).
- [50] P. G. Saffman, *Vortex Dynamics*, Cambridge Monographs on Mechanics (Cambridge University Press, 1993).
- [51] J. Huang and L. Fauci, Interaction of toroidal swimmers in stokes flow, *Physical Review E* **95**, 043102 (2017).
- [52] M. Chatzimanolakis, *High Performance Computing of Vortex Dominated Flows with Adaptive Mesh Refinement*, Ph.D. thesis, ETH Zurich (2023).
- [53] M. Gazzola, M. Argentina, and L. Mahadevan, Scaling macroscopic aquatic locomotion, *Nature Physics* **10**, 758 (2014).

- [54] J. P. Hernandez-Ortiz, C. G. Stoltz, and M. D. Graham, Transport and collective dynamics in suspensions of confined swimming particles, *Physical Review Letters* **95**, 204501 (2005).

Appendix A: Phase diagrams for three-dimensional model

This appendix contains the phase diagrams for the planar dynamics of a pair of three-dimensional source-sink swimmers with $\Delta\theta \neq 0$. Symbols and colors are as in Figure 10.

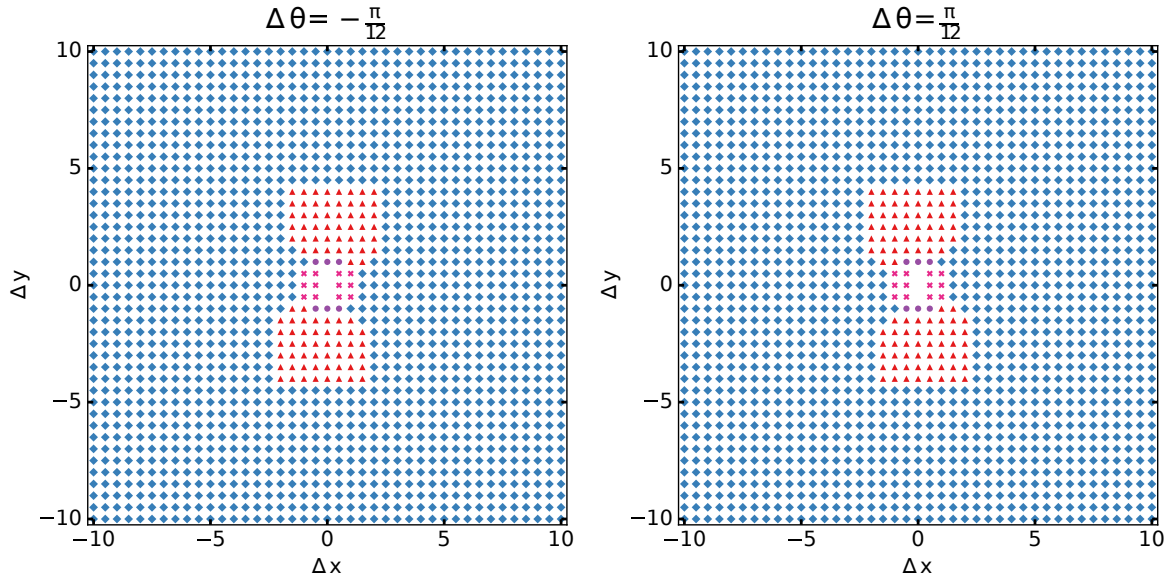


FIG. A.1. Phase diagrams for $|\Delta\theta| = \frac{\pi}{12}$ for three-dimensional swimmers.

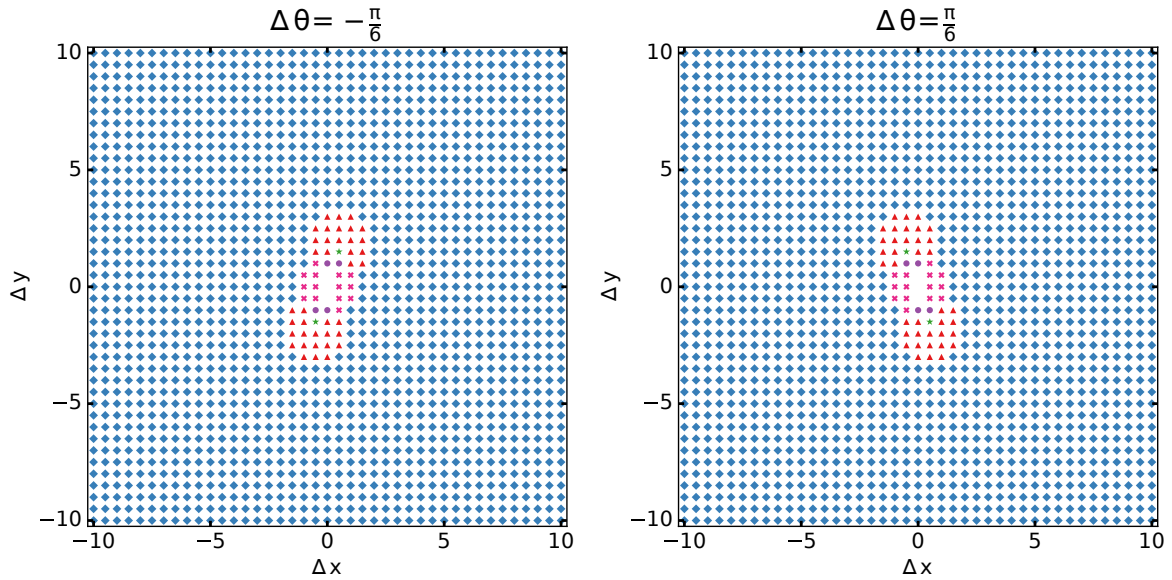


FIG. A.2. Phase diagrams for $|\Delta\theta| = \frac{\pi}{6}$ for three-dimensional swimmers.

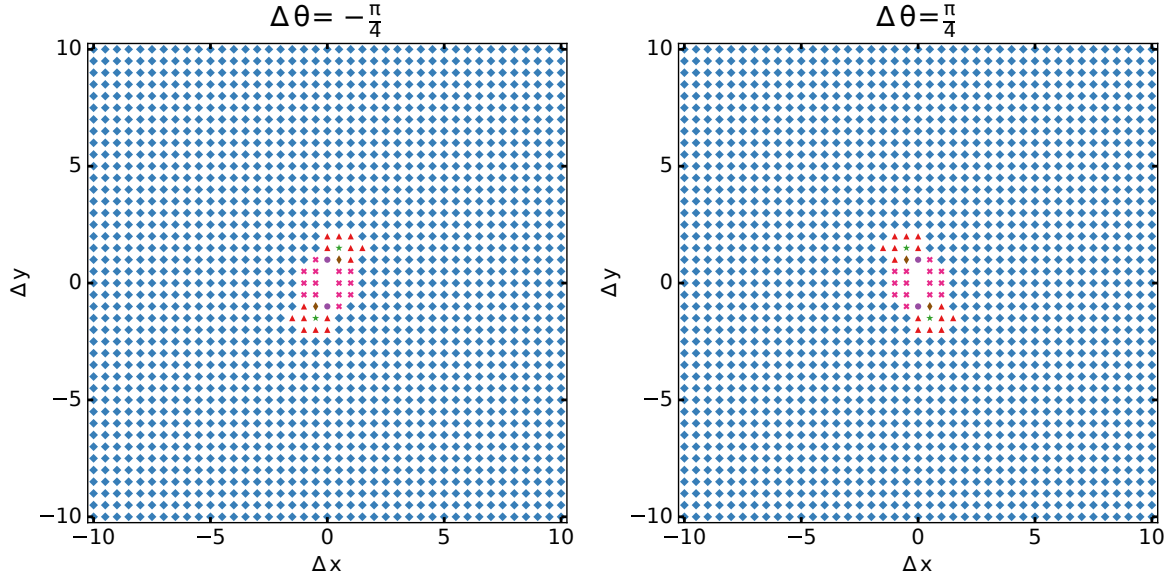


FIG. A.3. Phase diagrams for $|\Delta\theta| = \frac{\pi}{4}$ for three-dimensional swimmers.

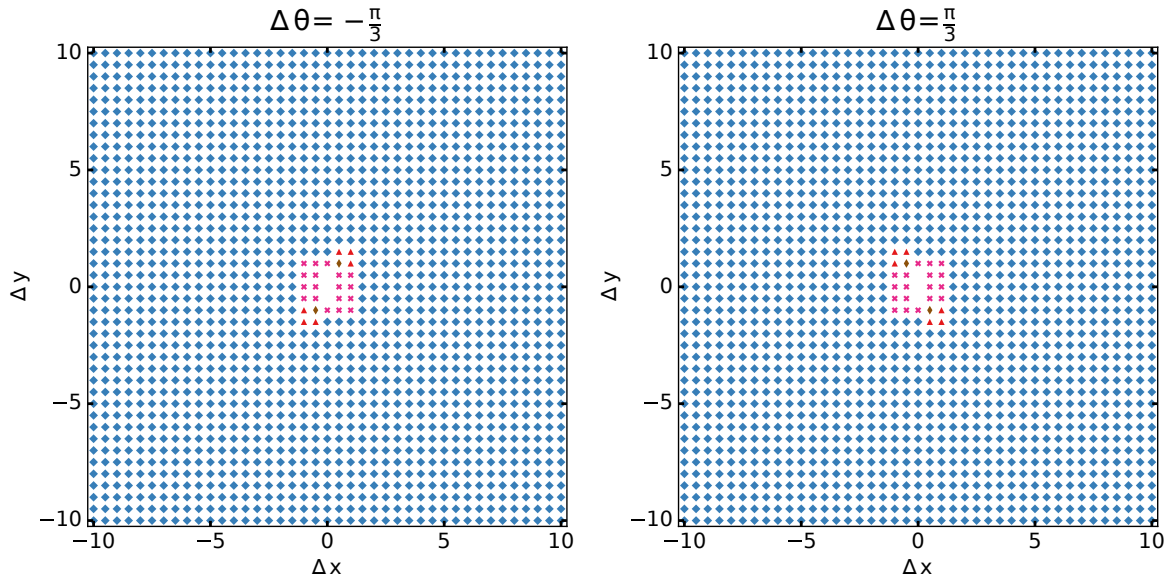


FIG. A.4. Phase diagrams for $|\Delta\theta| = \frac{\pi}{3}$ for three-dimensional swimmers.

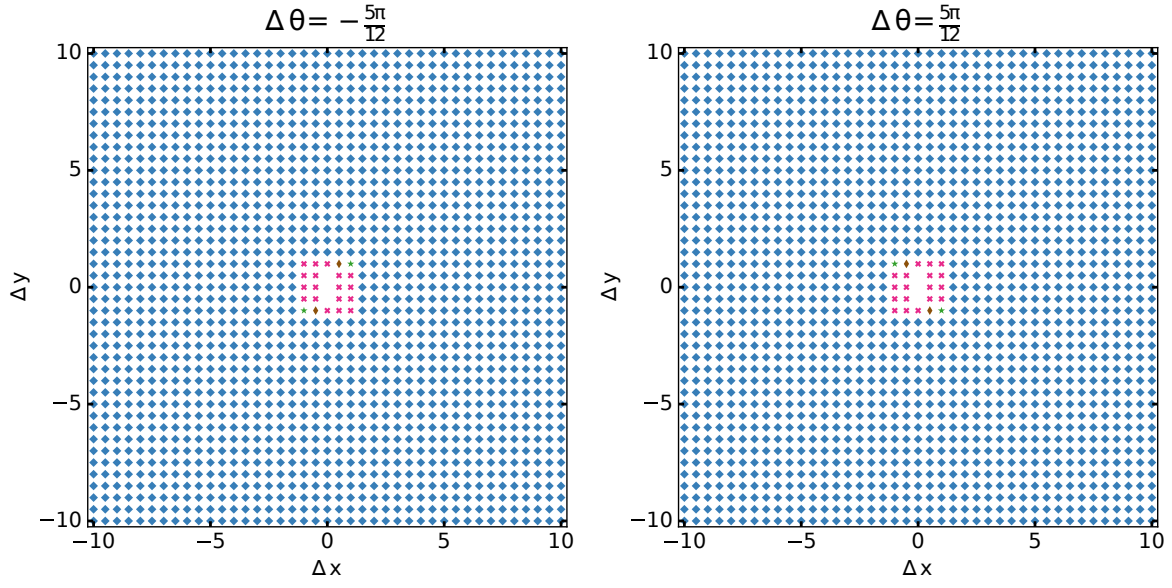


FIG. A.5. Phase diagrams for $|\Delta\theta| = \frac{5\pi}{12}$ for three-dimensional swimmers.

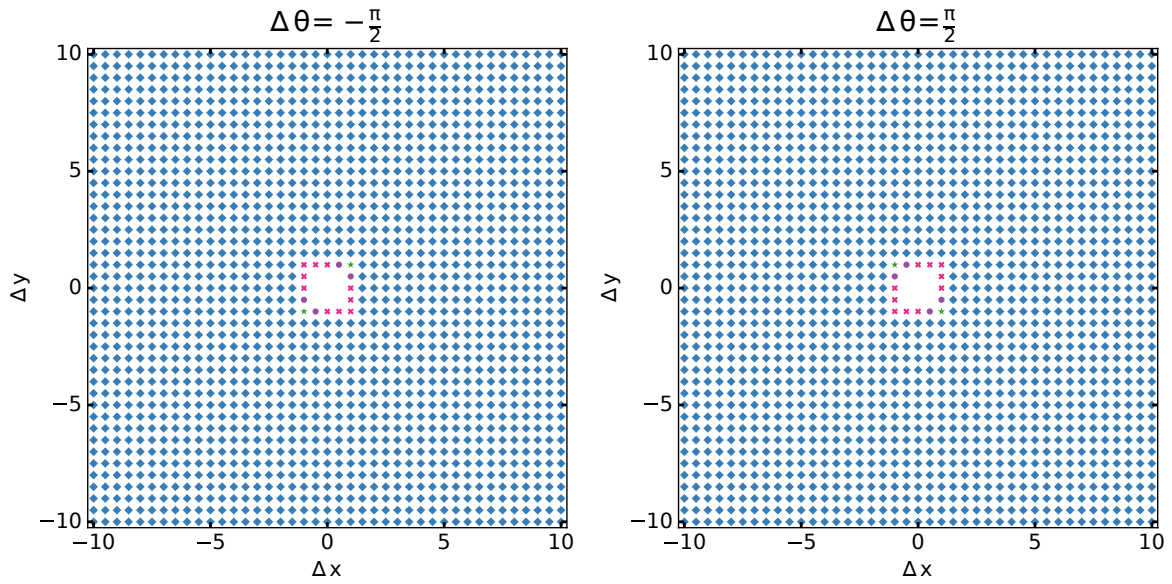


FIG. A.6. Phase diagrams for $|\Delta\theta| = \frac{\pi}{2}$ for three-dimensional swimmers.

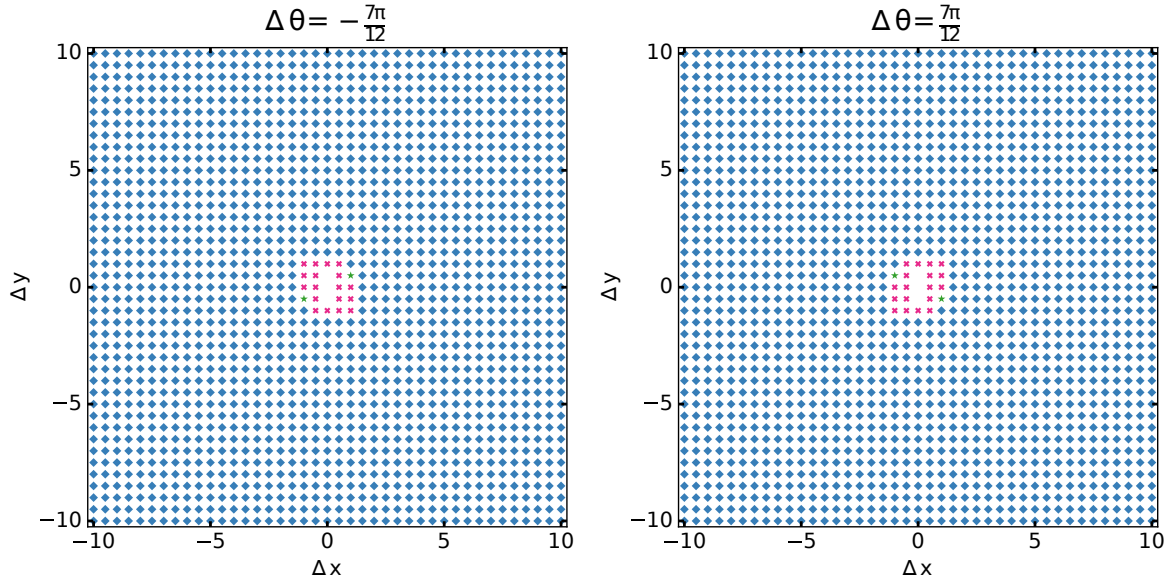


FIG. A.7. Phase diagrams for $|\Delta\theta| = \frac{7\pi}{12}$ for three-dimensional swimmers.

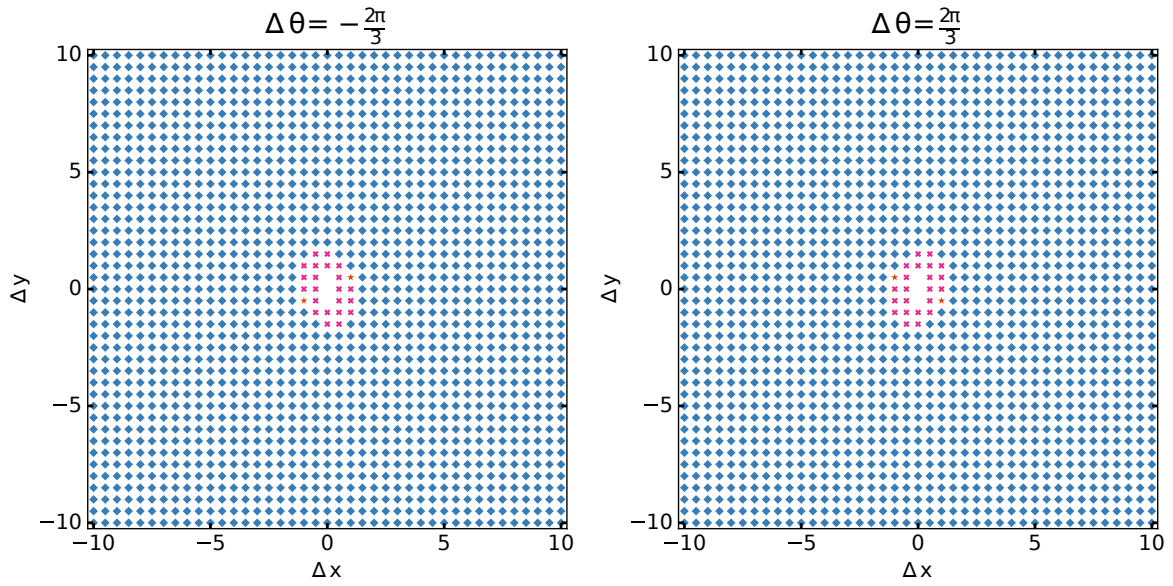


FIG. A.8. Phase diagrams for $|\Delta\theta| = \frac{2\pi}{3}$ for three-dimensional swimmers.

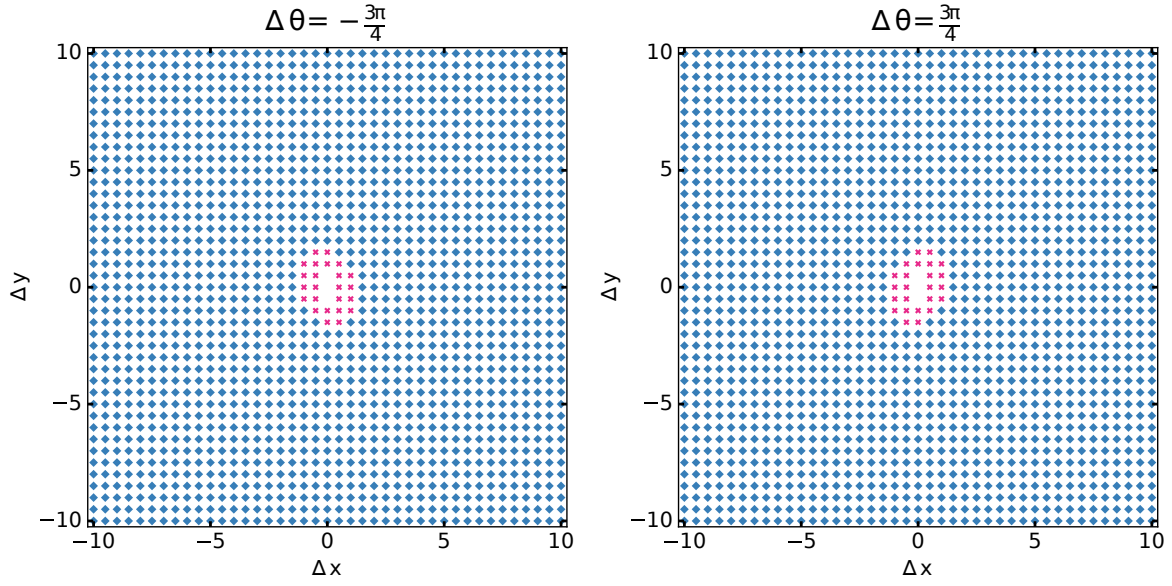


FIG. A.9. Phase diagrams for $|\Delta\theta| = \frac{3\pi}{4}$ for three-dimensional swimmers.

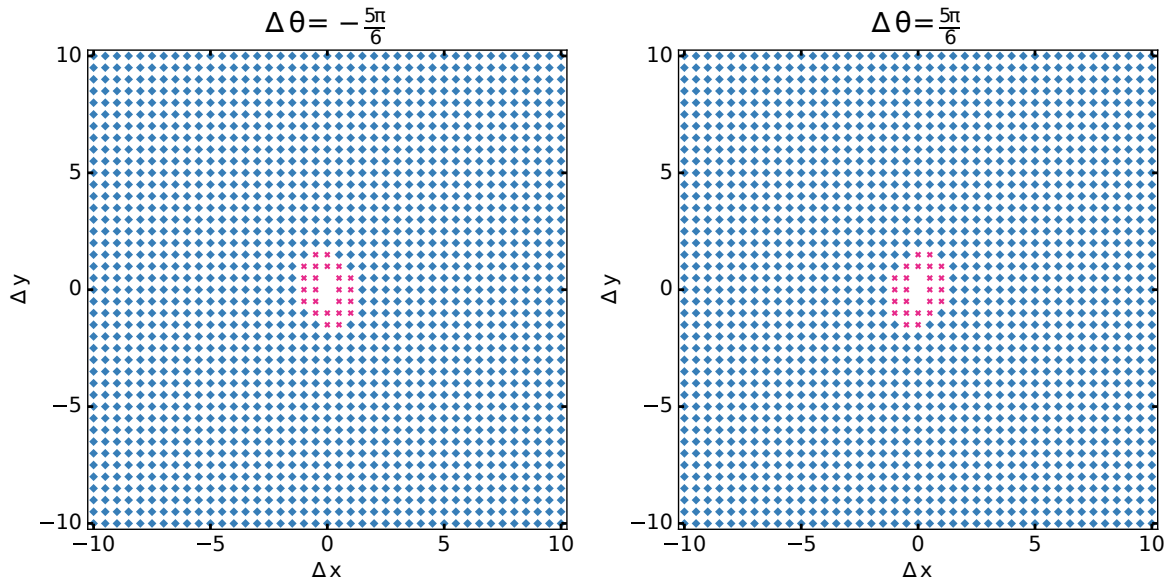


FIG. A.10. Phase diagrams for $|\Delta\theta| = \frac{5\pi}{6}$ for three-dimensional swimmers.

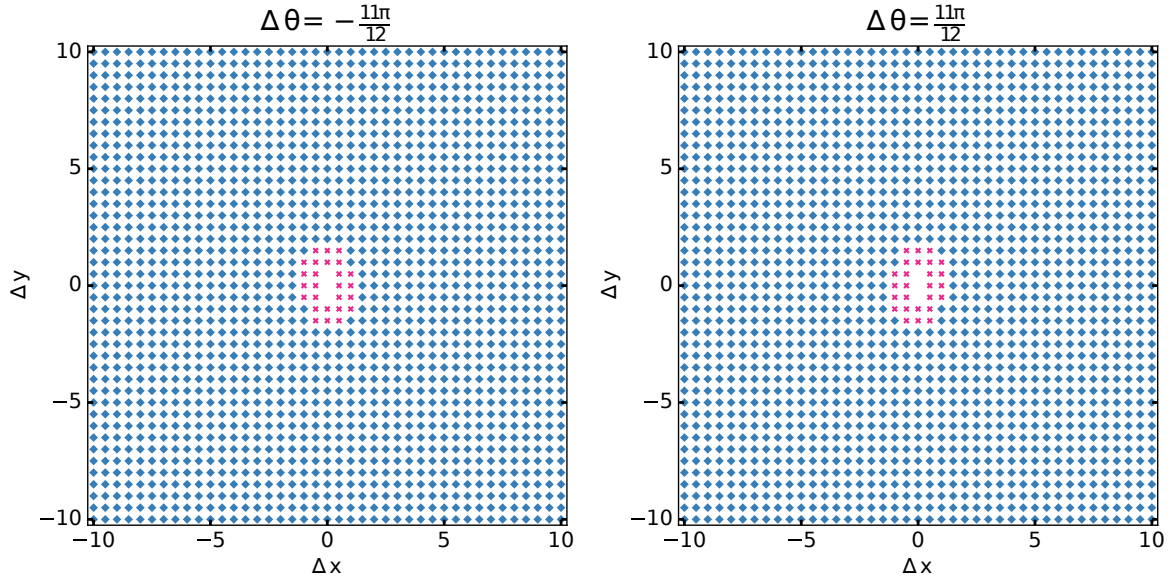


FIG. A.11. Phase diagrams for $|\Delta\theta| = \frac{11\pi}{12}$ for three-dimensional swimmers.

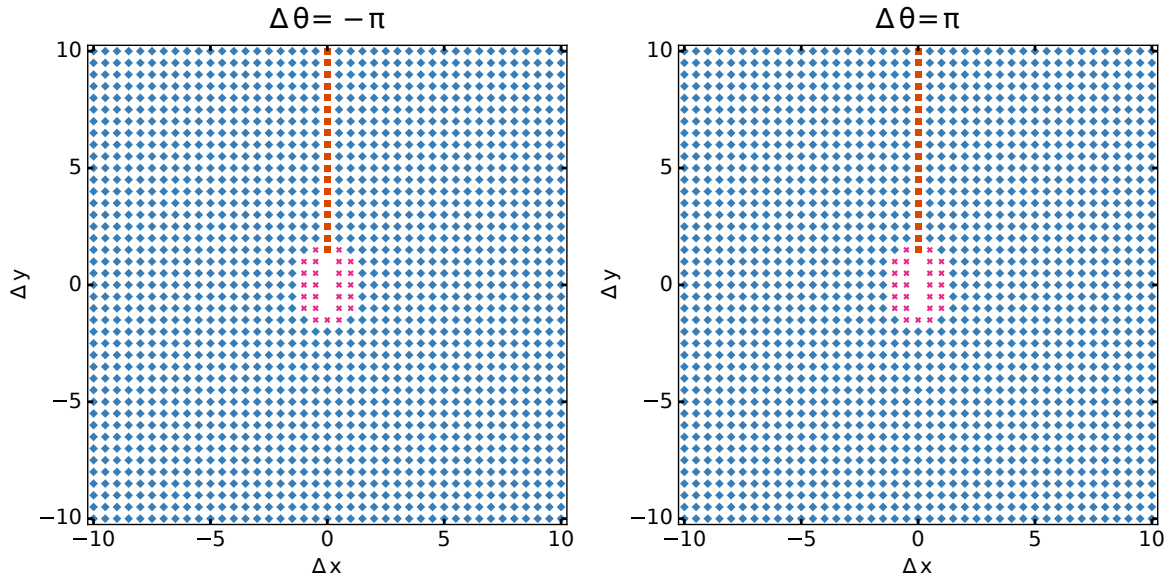


FIG. A.12. Phase diagrams for $|\Delta\theta| = \pi$ for three-dimensional swimmers.

Appendix B: Phase diagrams for two-dimensional model

This appendix contains the phase diagrams for the planar dynamics of a pair of two-dimensional source-sink swimmers with $\Delta\theta \neq 0$. Symbols and colors are as in Figure 14.

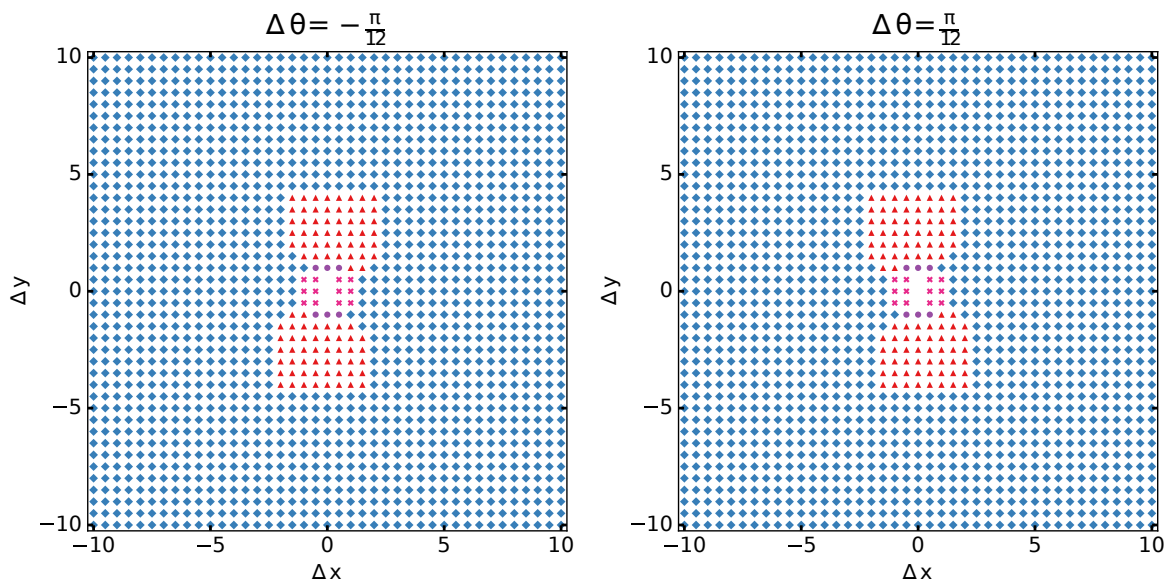


FIG. B.1. Phase diagrams for $|\Delta\theta| = \frac{\pi}{12}$ for two-dimensional swimmers.

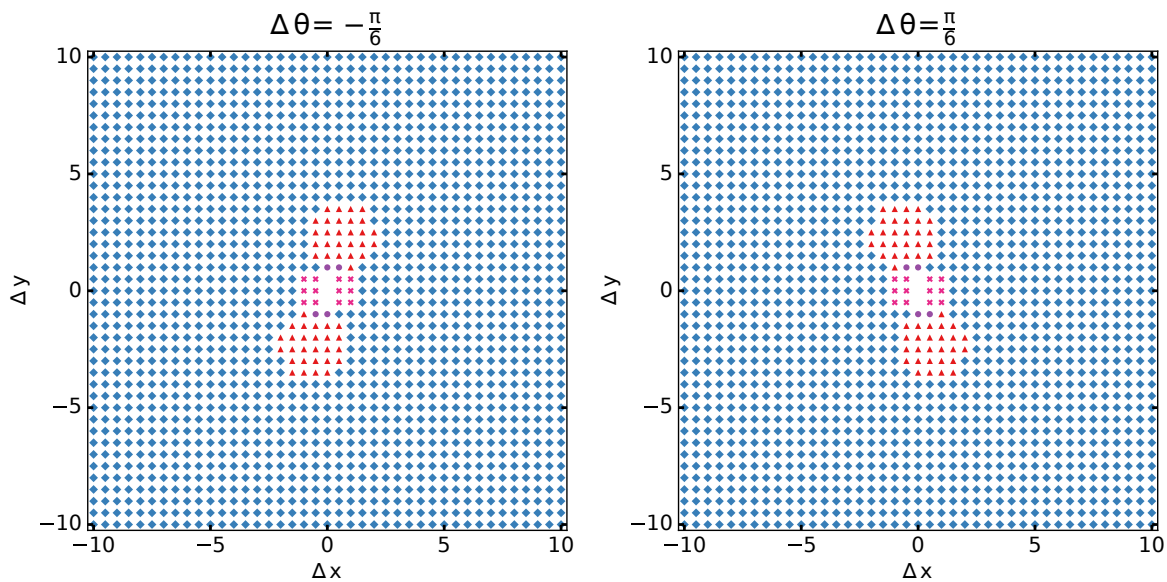


FIG. B.2. Phase diagrams for $|\Delta\theta| = \frac{\pi}{6}$ for two-dimensional swimmers.

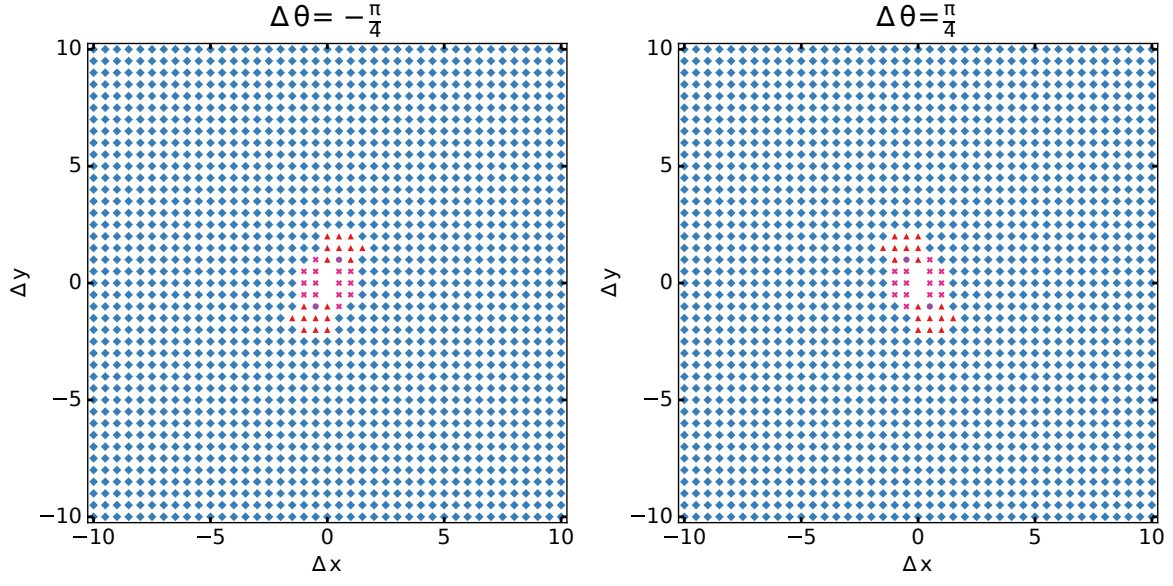


FIG. B.3. Phase diagrams for $|\Delta\theta| = \frac{\pi}{4}$ for two-dimensional swimmers.

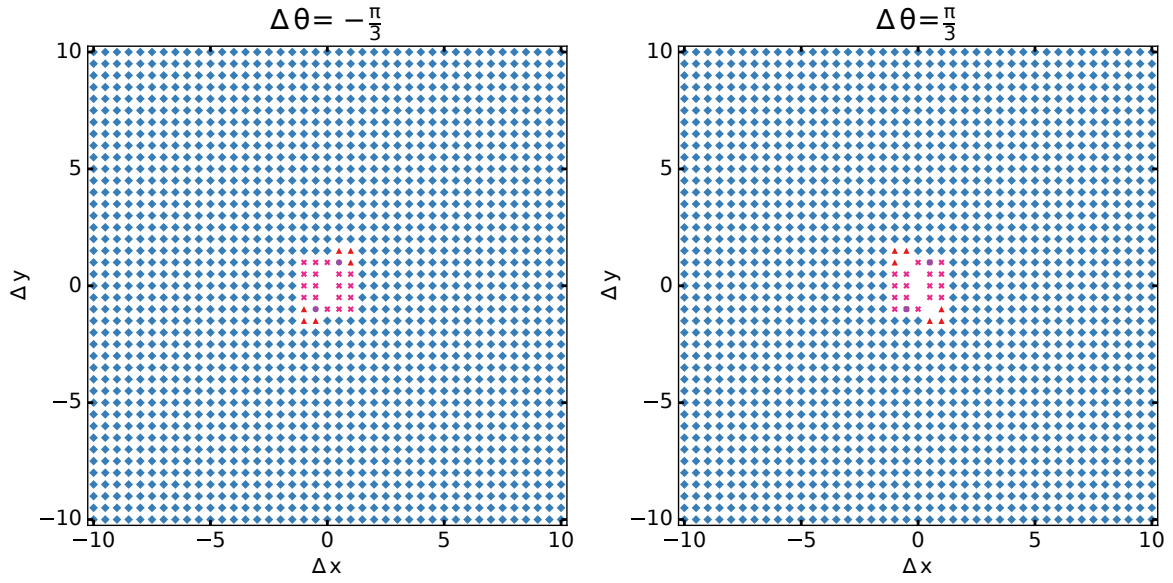


FIG. B.4. Phase diagrams for $|\Delta\theta| = \frac{\pi}{3}$ for two-dimensional swimmers.

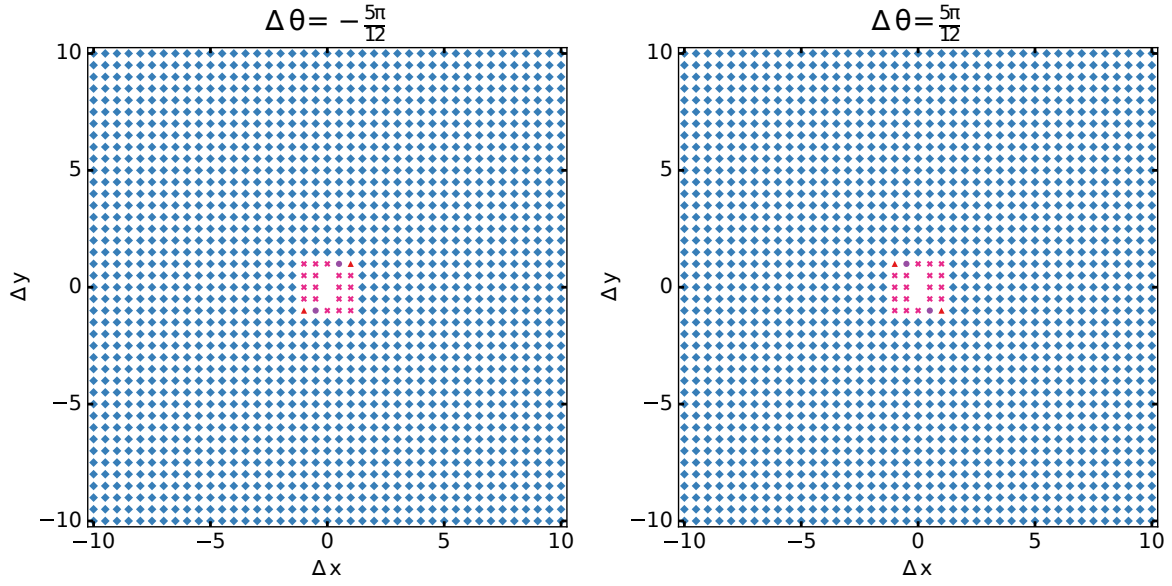


FIG. B.5. Phase diagrams for $|\Delta\theta| = \frac{5\pi}{12}$ for two-dimensional swimmers.

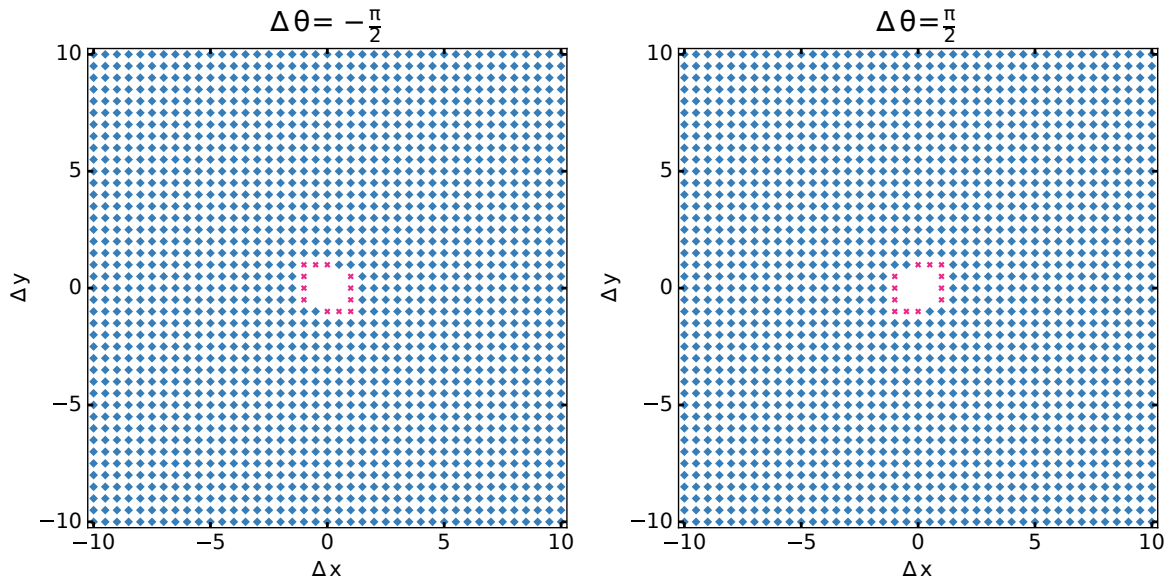


FIG. B.6. Phase diagrams for $|\Delta\theta| = \frac{\pi}{2}$ for two-dimensional swimmers.

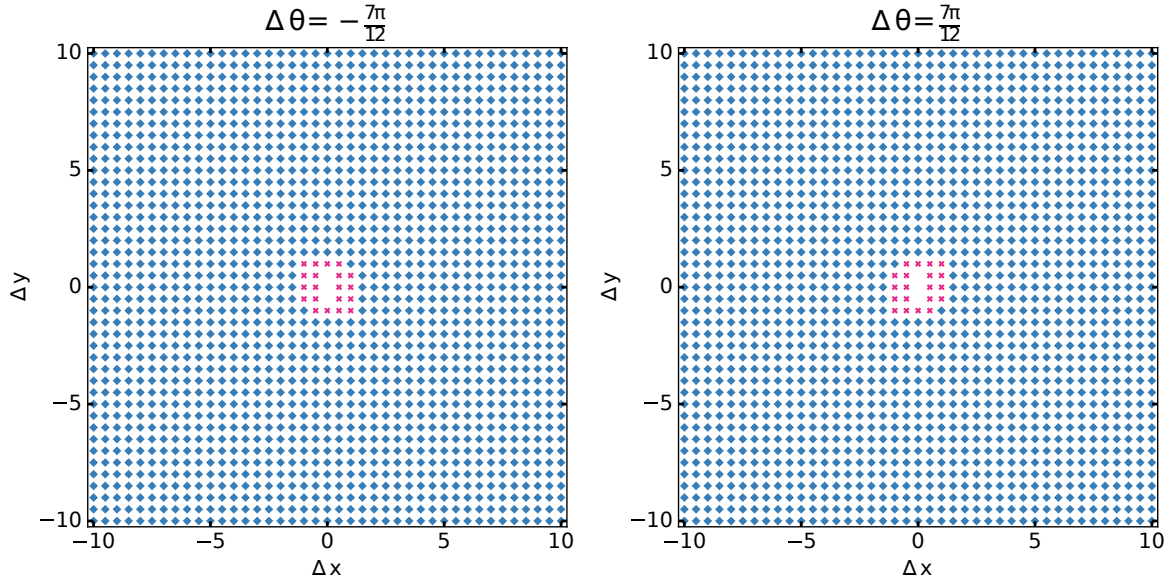


FIG. B.7. Phase diagrams for $|\Delta\theta| = \frac{7\pi}{12}$ for two-dimensional swimmers.

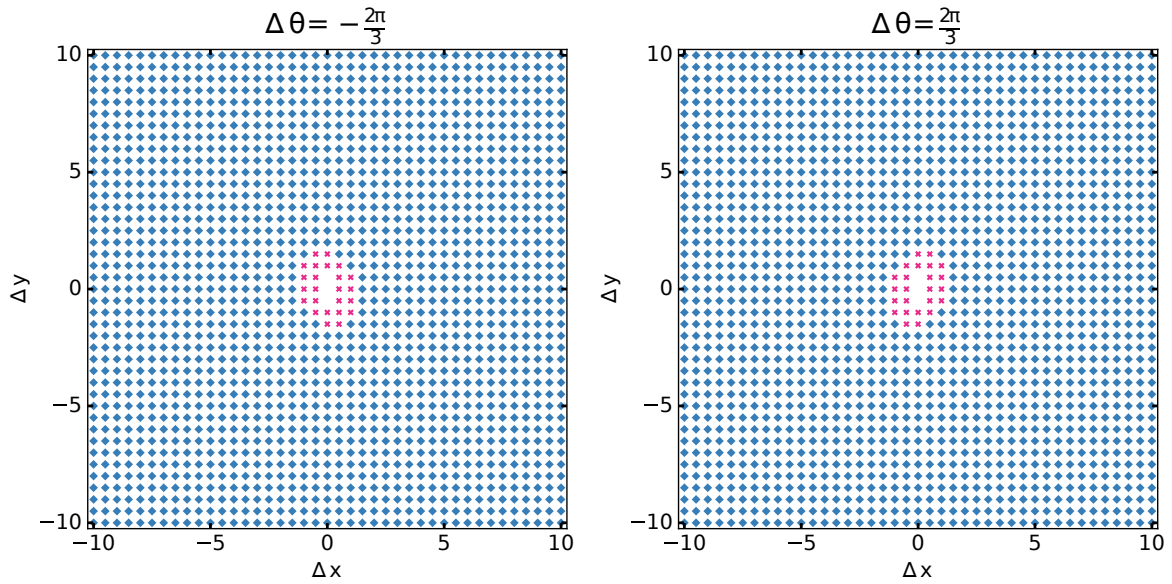


FIG. B.8. Phase diagrams for $|\Delta\theta| = \frac{2\pi}{3}$ for two-dimensional swimmers.

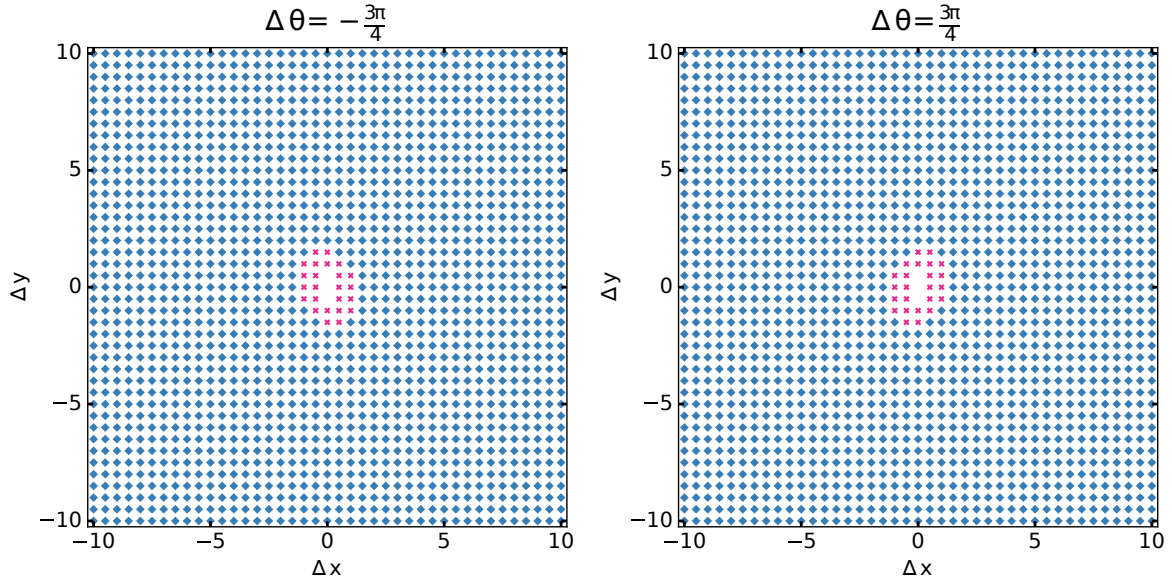


FIG. B.9. Phase diagrams for $|\Delta\theta| = \frac{3\pi}{4}$ for two-dimensional swimmers.

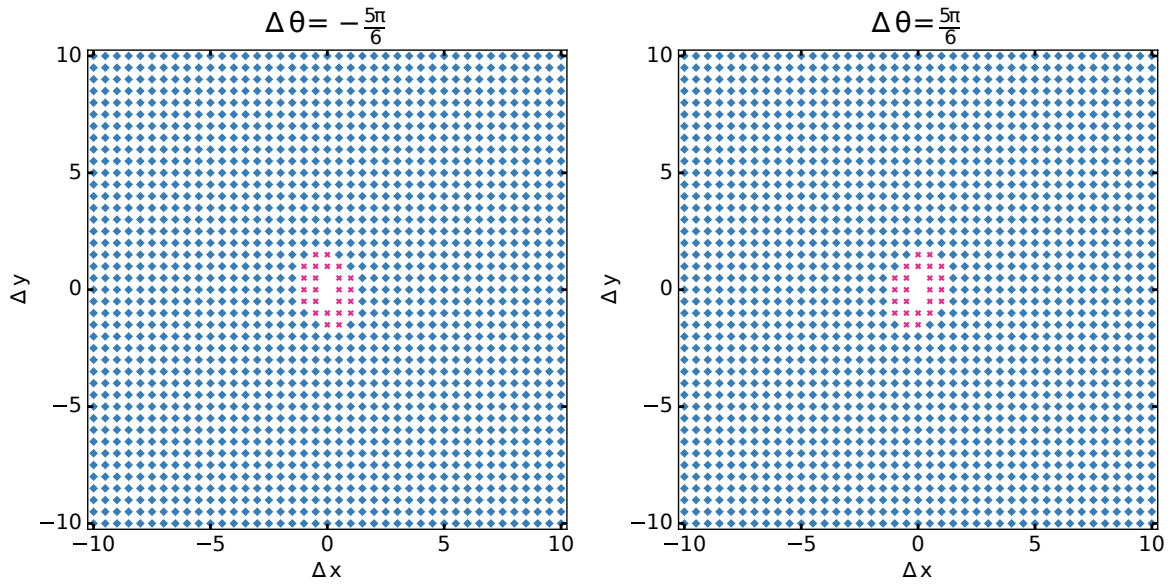


FIG. B.10. Phase diagrams for $|\Delta\theta| = \frac{5\pi}{6}$ for two-dimensional swimmers.

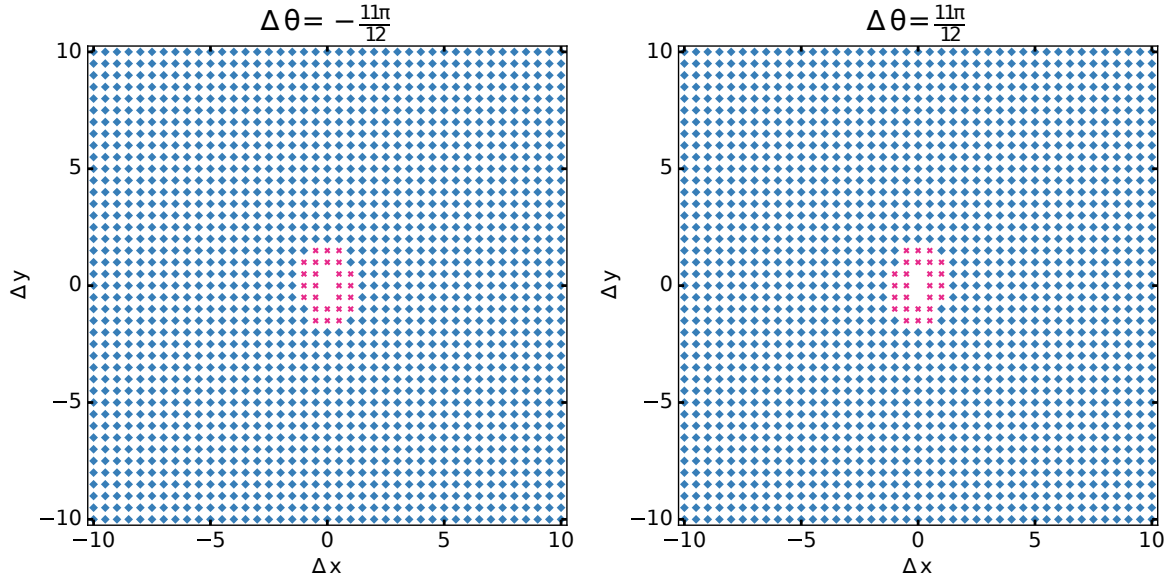


FIG. B.11. Phase diagrams for $|\Delta\theta| = \frac{11\pi}{12}$ for two-dimensional swimmers.

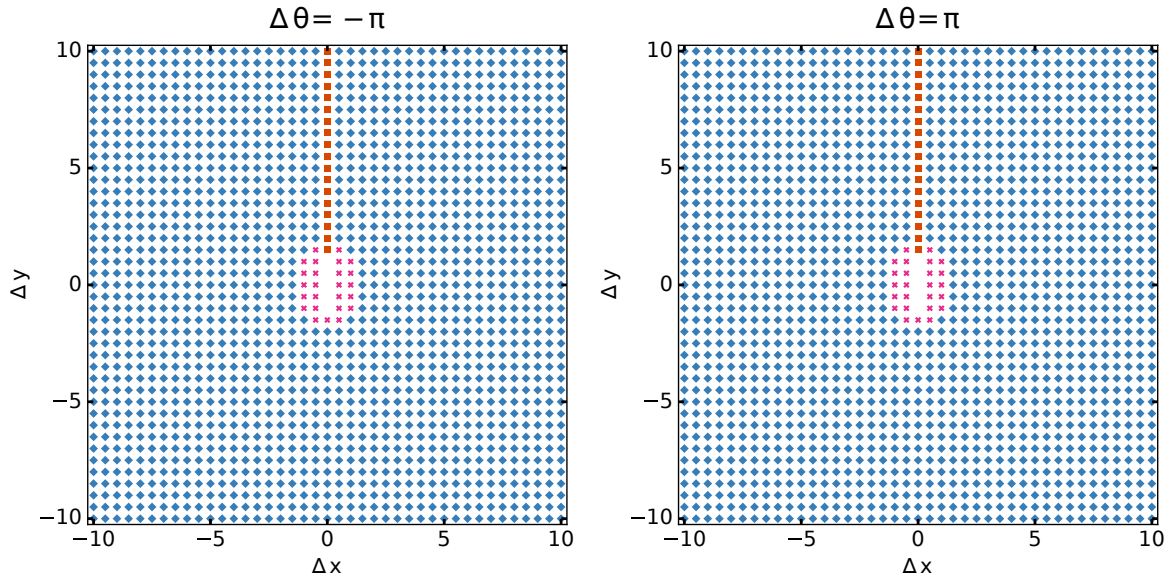


FIG. B.12. Phase diagrams for $|\Delta\theta| = \pi$ for two-dimensional swimmers.